研究成果の刊行に関する一覧表

雑誌

発表者の氏名	論文タイトル名	発表誌名	巻号	ページ	出版年
Horiba et al.	Cloning and characterization of a novel Na^+-dependent glucose transporter (NaGLT1) in rat kidney	J. Biol. Chem.	278(17)	14669 -14676	2003
Horiba et al.	Na^+-dependent fructose transport via rNaGT1 in rat kidney	FEBS Lett.	546(2-3)	276 -280	2003
Pan et al.	Altered diurnal rhythm of intestinal peptide transporter by fasting and its effects on the pharmacokinetics of ceftibuten	J. Pharmacol. Exp. Ther.	307(2)	626 -632	2003
Takeuchi et al.	Decreased function of genetic variants, Pro283Leu and Arg287Gly, in human organic cation transporter hOCT1	Drug Metabol. Pharmacokin.	18(6)	409 -412	2003
Sakurai et al.	Expression levels of renal organic anion transporters (OATs) and their correlation with anionic drug excretion in patients with renal diseases	Pharm. Res.	21(1)	61-67	2004
Terada et al.	Genetic variant Arg57His in human H^+/peptide cotransporter 2 causes a complete loss of transport function	Biochem. Biophys. Res. Commun.	316(2)	416 -420	2004
Uwai et al.	Common single nucleotide polymorphisms of MDR1 gene have no influence on its mRNA expression levels of nomal kidney cortex and renal cell carcinoma in Japanese nephrectomized patients	J. Hum. Genet.	49(1)	40-45	2004
Terada et al.	Peptide transporters: structure, function, regulation and application for drug delivery	Curr. Drug Metab.	5(1)	85-94	2004
Urakami et al.	Creatinine transport by basolateral organic cation transporter hOCT2 in the human kidney.	Pharm. Res.	21(6)	982 -987	2004
Horiba et al.	Gene expression variance based on random sequencing in rat remnant kidney.	Kidney Int.	66(1)	29-45	2004
Motohashi et al.	Different transport properties between famotidine and cimetidine by human renal organic ion transporters (SLC22A).	Eur. J. Pharmacol.,	503(1-3)	25-30	2004
Kimura et al.	Metformin Transport by Renal Basolateral Organic Cation Transporter hOCT2.	Pharm. Res.,	22(2)	255 -259	2005

THE JOURNAL OF BIOLOGICAL CHEMISTRY
Vol. 278, No. 17, Issue of April 25, pp. 14669–14676, 2003
Printed in U.S.A.

Cloning and Characterization of a Novel Na^+-dependent Glucose Transporter (NaGLT1) in Rat Kidney*

Received for publication, December 2, 2002, and in revised form, January 29, 2003
Published, JBC Papers in Press, February 14, 2003, DOI 10.1074/jbc.M212240200

Naoshi Horiba, Satohiro Masuda, Ayako Takeuchi, Daisuke Takeuchi, Masahiro Okuda, and Ken-ichi Inui‡

From the Department of Pharmacy, Kyoto University Hospital, Faculty of Medicine, Kyoto University, Sakyo-ku, Kyoto 606-8507, Japan

To identify novel transporters in the kidney, we have constructed an mRNA data base composed of 1000 overall clones by random sequencing of a male rat kidney cDNA library. After a BLAST search, ~40% of the clones were unknown and/or unannotated and were screened by measuring the uptake of various compounds using *Xenopus* oocytes. One clone stimulated the uptake of α-methyl-D-glucopyranoside and therefore was termed rat Na^+-dependent glucose transporter 1 (rNaGLT1). The rNaGLT1 cDNA (2173 bp) has an open reading frame encoding a 484-amino acid protein, showing <22% homology to known SGLT and GLUT glucose transporters. α-Methyl-D-glucopyranoside uptake by rNaGLT1 cRNA-injected oocytes showed saturability, with an apparent K_m of 3.7 mM and a coupling ratio of 1:1 with Na^+. rNaGLT1 mRNA was expressed predominantly in the kidney upon Northern blot analysis and reverse transcription-PCR. Reverse transcription-PCR in microdissected nephron segments revealed that rNaGLT1 mRNA was primarily localized in the proximal tubules. A clear signal corresponding to rNaGLT1 protein was recognized in the brush-border (but not basolateral) membrane fraction by immunoblot analysis. The rNaGLT1 mRNA level in the kidney was significantly higher than rat SGLT1 and SGLT2 mRNA levels. These findings suggest that rNaGLT1 is a novel Na^+-dependent glucose transporter with low substrate affinity that mediates tubular reabsorption of glucose.

Recently, several high throughput DNA sequencing approaches have been performed, such as the human genome project, the mouse genome project, and so on, in which many gene arrangements have been revealed and submitted to the DDBJ/GenBank™/EMBL Data Bank (1, 2). However, for a large number of them, only the nucleic acid and amino acid sequences have been clarified, with little information available concerning their functions and tissue distributions. It is conceivable to assume that there are many unknown transporters among these unknown/unannotated genes. Although some transporters have been isolated recently using the nucleotide sequences in the expressed sequence tag data bases, most of them are members of known transporter families (3, 4), suggesting difficulty in identifying novel transporter genes.

The random sequencing of a cDNA library, in which several thousand clones are randomly picked and sequenced, is one of the promising methods of establishing mRNA expression data bases (5). The mRNAs in a data base constructed from the mouse kidney using this method can be considered to be abundantly expressed and physiologically significant *in vivo* (6–8). However, ~70% of the clones identified by this method were unknown cDNAs that were not submitted to the DDBJ/GenBank™/EMBL Data Bank or that were submitted with only the base or amino acid sequences to the mouse kidney cDNA data base (6). As the transporter-related mRNAs share >2% of the known mRNAs in these studies (6, 7), some novel transporter-related mRNAs might exist among unknown mRNAs. Based on this hypothesis, we constructed an mRNA data base of male rat kidney and screened unknown genes in the data base by measuring the uptake of various compounds using *Xenopus* oocytes. Consequently, we found a novel Na^+-dependent glucose transporter (rNaGLT1)[1] that transports α-methyl-D-glucopyranoside (α-MeGlc) in an Na^+-dependent manner.

Glucose is reabsorbed in renal proximal tubules by several hexose transporters (9). To date, two Na^+-dependent glucose transporters, SGLT1 (10) and SGLT2 (11, 12), with high and low affinity for their substrates, respectively, have been isolated from intestine or kidney. SGLT2 is predominantly expressed in the S1 segment of proximal tubules, whereas SGLT1 is present in the S3 segment. It is generally accepted that SGLT1 and SGLT2 work cooperatively during the reabsorption of glucose in the proximal tubules. Although the severe glucose/galactose malabsorption disease is caused by a single missense mutation of the SGLT1 nucleotide sequence in the small intestine, slight glycosuria is observed in patients with this disease (13). This finding indicates that SGLT1 may play a small part in the reabsorption of glucose in the kidney (9). In addition, there are few studies suggesting mutations of SGLT2 accompanying a severe inherited disease. It has been speculated that Fanconi's syndrome or primary renal glycosuria involves a malfunction of renal glucose transporters. Although Santer *et al.* (14) have suggested the involvement of GLUT2 in Fanconi's syndrome, the mechanisms inducing renal glycosuria remain largely to be clarified (9). In this study, we report the cDNA cloning of a novel Na^+-dependent glucose transporter (rNa-

* This work was supported by Grant-in-aid for Research on Human Genome, Tissue Engineering, and Food Biotechnology H12-Genome-019 from the Ministry of Health, Labor, and Welfare of Japan and by a grant-in-aid for scientific research from the Ministry of Education, Culture, Sports, Science, and Technology of Japan. The costs of publication of this article were defrayed in part by the payment of page charges. This article must therefore be hereby marked "*advertisement*" in accordance with 18 U.S.C. Section 1734 solely to indicate this fact.

The nucleotide sequence(s) reported in this paper has been submitted to the GenBank™/EBI Data Bank with accession number(s) AB089802.

‡ To whom correspondence should be addressed. Tel.: 81-75-751-3577; Fax: 81-75-751-4207; E-mail: inui@kuhp.kyoto-u.ac.jp.

[1] The abbreviations used are: rNaGLT1, rat Na^+-dependent glucose transporter 1; α-MeGlc, α-methyl-D-glucopyranoside; rSGLT, rat sodium-dependent glucose transporter; GLUT, glucose transporter; 2-DG, 2-deoxy-D-glucose; RT, reverse transcription; rGAPDH, rat glyceraldehyde-3-phosphate dehydrogenase.

TABLE I

Oligonucleotide sequences of PCR primers used for the determination of glucose transporters and rGAPDH by RT-PCR and Northern blotting

RT-PCR and Northern blotting were performed as described under "Experimental Procedures." Positions are from the rat sequence in the GenBank ™/EBI Data Bank, and the accession numbers are indicated.

Primer	Sequence	Positions
rNaGLT1 (AB089802)		
Forward	5′-TGGGACCCACATTTCCAGAC-3′	279–298
Reverse	5′-TCTGAGGCGGCTTCAAAGGATC-3′	736–757
rSGLT1 (D16101)		
Forward	5′-ATGGACAGTAGCACCTTGAGCC-3′	170–191
Reverse	5′-TAGCCCCAGAGAAGATGTCTGC-3′	647–668
rSGLT2 (U29881)		
Forward	5′-CATTGTCTCAGGCTGGCACTGG-3′	851–872
Reverse	5′-GGACACTGCCACAATGAACACC-3′	1289–1310
rGAPDH (M17701)		
Forward	5′-CCTTCATTGACCTCAACTAC-3′	131–150
Reverse	5′-GGAAGGCCATGCCAGTGAGC-3′	705–724

GLT1) that would play a critical role in the tubular reabsorption of glucose.

EXPERIMENTAL PROCEDURES

Materials—α-[U-^{14}C]MeGlc (11.7 GBq/mmol), D-[1-^{14}C]galactose (2.07 GBq/mmol), and D-[U-^{14}C]mannose (11.6 GBq/mmol) were obtained from Amersham Biosciences (Uppsala, Sweden). D-[1-^{3}H]Mannitol (629 GBq/mmol), [^{3}H]digoxin (584.6 GBq/mmol), 1-[^{3}H]methyl-4-phenylpyridinium acetate (2886 GBq/mmol), [6,7-^{3}H]estrone sulfate (1609 GBq/mmol), [^{14}C]glycylsarcosine (1.848 GBq/mmol), and L-[^{3}H]leucine (1573 GBq/mmol) were obtained from PerkinElmer Life Sciences. D-[^{3}H]Glucose (566.1 GBq/mmol), 2-[1,2-^{3}H]deoxy-D-glucose (2-DG; 925 GBq/mmol), and L-[2,5-^{3}H]histidine (1628 GBq/mmol) were purchased from Moravek Biochemicals, Inc. (Brea, CA). [9-^{3}H]Quinidine (740 GBq/mmol) was purchased from American Radiolabeled Chemicals (St. Louis, MO). [^{14}C]Ciprofloxacin hydrochloride (2.55 GBq/mmol) was a gift from Bayer AG (Leverkusen-Bayerwerk, Germany). Phlorizin, α-MeGlc, D-glucose, L-glucose, D-galactose, D-mannose, D-fructose, and D-mannitol were purchased from Nacalai Tesque, Inc. (Kyoto, Japan). Phloretin and 2-DG were obtained from Sigma. All other chemicals were of the highest purity available.

Construction of a cDNA Library from Rat Kidney mRNA and Its Screening—Total RNA was extracted from the kidneys of 9-week-old male rats (n = 6) by the guanidine isothiocyanate/CsCl ultracentrifugation method. The poly(A)$^+$ RNA was purified by chromatography on an oligo(dT)-cellulose affinity column (Stratagene, La Jolla, CA) as described previously (15). The cDNA library was constructed using the λZaP Express cDNA synthesis kit (Stratagene) according to the manufacturer's instructions. After conversion from phage to plasmid, 1000 colonies were randomly chosen from this cDNA library and sequenced using the RISA-384 multicapillary DNA sequencing system (Shimadzu, Kyoto) from the 5′-end with primer T3. The resulting sequences were submitted to a BLAST search of the DDBJ/GenBank™/EMBL Data Bank and the Protein Data Bank. Four-hundred unknown clones from the rat kidney cDNA library were subjected to a BLAST search. These clones were screened for the transport activity of nine compounds using *Xenopus* oocytes.

Microdissection of Rat Nephrons—Rat nephrons were microdissected as described previously (16). Briefly, the left kidneys of 7-week-old rats weighing 140–160 g were perfused and removed. Slices were cut along the medullary axis and incubated with collagenase. The tubules were microdissected to obtain the following structures: glomerulus, proximal convoluted tubule, proximal straight tubule, medullary thick ascending limb, cortical thick ascending limb, cortical collecting duct, outer medullary collecting duct, and inner medullary collecting duct. After microdissection, 20 glomeruli and 8 mm of each dissected tubule segment were transferred into tubes to isolate total RNA using an RNeasy® minikit (QIAGEN Inc., Hilden, Germany).

Reverse Transcription (RT)-PCR Analysis—Total RNA from the dissected tubules or poly(A)$^+$ RNA from rat tissues (brain, heart, lung, liver, small intestine, spleen, kidney cortex, and kidney medulla) was reverse-transcribed with random hexamers using Superscript II reverse transcriptase (Invitrogen), followed by RNase H (Invitrogen) digestion. These single-stranded DNA fragments were amplified with primer sets specific for rNaGLT1, rSGLT1, rSGLT2, and rat glyceraldehyde-3-phosphate dehydrogenase (rGAPDH), as shown in Table I.

Northern Blot Analysis—Five micrograms of total RNA from rat kidney or 1 μg of poly(A)$^+$ RNA from the eight tissues was electrophoresed on 1% denaturing agarose gel containing formaldehyde and transferred onto Hybond® N$^+$ nylon membranes (Amersham Biosciences). The transferred RNAs were linked to the nylon membrane by a UV cross-linker. The quality of the RNA was assessed by ethidium bromide staining. After transfer, the blots were hybridized under high stringency conditions (50% formamide, 5× saline/sodium phosphate/EDTA (20 × saline/sodium phosphate/EDTA = 3 M NaCl, 0.2 M NaH_2PO_4, and 0.02 M EDTA, pH 7.4), 5× Denhardt's solution, 0.1% sodium dodecyl sulfate, and 10 μg/ml herring sperm DNA at 42 °C) with rNaGLT1, rSGLT1, rSGLT2, and rGAPDH cDNA fragments labeled with [α-^{32}P]dCTP (29.6 TBq/mmol; Amersham Biosciences). Each probe was obtained by RT-PCR amplification of rat kidney total RNA as described above (Table I). After hybridization, the blots were washed three times with 2× SSC (20× SSC = 3 M NaCl and 0.3 M sodium citrate, pH 7.0) containing 0.1% SDS at 42 °C for 10 min and then twice with 0.5× SSC and 0.1% SDS at 42 °C for 30 min. The dried membranes were exposed to the imaging plates of a Fujix BIO-imaging BAS-2000 II analyzer (Fuji Photo Film Co., Tokyo, Japan). To compare the expression levels of rNaGLT1 and rSGLT1 or rSGLT2, the experimental conditions (such as the quantity of labeled probes, the wash conditions, and the exposure time) were kept uniform.

Polyclonal Antibody against rNaGLT1—Polyclonal antibody was raised against the synthetic peptide corresponding to the intracellular domains near the C terminus (LPLDRKQEKSINSEGQ) of rNaGLT1. The peptide was synthesized with cysteine for its N terminus (purity of 92.0% upon high performance liquid chromatography; Sawady Technology Co., Ltd., Tokyo). A male Japanese White rabbit (2 kg) was immunized with 0.2 mg of conjugates emulsified with Freund's complete adjuvant. Booster shots of conjugates emulsified with Freund's incomplete adjuvant were injected every 2 weeks until the antibody was obtained. After each booster shot, blood was collected, and antibody production was determined by enzyme-linked immunosorbent assay. To verify the specificity of antibody against rNaGLT1 protein, *Xenopus* oocytes injected with rNaGLT1 cRNA were used in the immunohistochemical analysis. Capped cRNA from rNaGLT1 was transcribed from *Not*I-linearized pBK-CMV containing rNaGLT1 cDNA with T3 RNA polymerase as described previously (17). Oocytes were injected with water (50 nl) or rNaGLT1 cRNA (25 ng). Three days after injection, oocytes were fixed with 4% paraformaldehyde in phosphate-buffered saline. Fixed oocytes were embedded in O.C.T. compound (Sakura Finetechnical, Tokyo) and rapidly frozen at −20 °C. Tissues were cut into 12-μm-thick sections, mounted on glass slides, and covered with 10% goat serum for 1 h. The covered sections were incubated with anti-rNaGLT1 serum (1:500 dilution) with or without preabsorption by the synthesized antigen peptide (50 μg/ml) for 1 h and then incubated with Cy3-labeled anti-rabbit IgG (Caltag Laboratories, San Francisco, CA) for 1 h. These sections were examined with a BX-50-FLA fluorescence microscope (Olympus, Tokyo) at magnification ×100. Images were captured with a DP-50 CCD camera (Olympus) using Studio Lite software (Olympus).

Immunoblot Analysis—Crude plasma membrane fractions were prepared from rat kidney cortex as reported previously (18). The brush-border and basolateral membrane fractions were obtained from rat renal cortex as described previously (19, 20). To carry out immunoblot analysis, the membrane fractions were solubilized in sample buffer (2% SDS, 125 mM Tris, and 20% glycerol) in the presence or absence of 50 mM dithiothreitol and heated at 95 °C for 10 min. The samples were separated by 10% SDS-PAGE and transferred to polyvinylidene diflu-

TABLE II
Nucleotide sequences of the primers and probes used for real-time PCR

Real-time PCR was performed as described under "Experimental Procedures." Positions are from the rat sequence in the GenBank™/EBI Data Bank, and accession numbers are indicated.

Primer		Positions
rNaGLT1 (AB089802)		
Forward	5′-CCGGTGTCTCATTTGGTGTTCT-3′	526–547
Reverse	5′-ACCCAAGGCGAAACTGAAGTG-3′	618–638
TaqMan probe	5′-ACAAAGGAGCCCCACATATTCAGGCCTT-3′	589–616
rSGLT1 (D16101)		
Forward	5′-CGAGGAGGACCCTAAAGATACCA-3′	1912–1934
Reverse	5′-GAACAGGTCATATGCCTTCCTGA-3′	1977–1999
TaqMan probe	5′-TGAAATAGATGCAGAAGCCCCCCAGAAGG-3′	1936–1964
rSGLT2 (U29881)		
Forward	5′-AAAATACGGCAGGAAGGAACTG-3′	2117–2138
Reverse	5′-GACAAATTGGCCACCATCTTG-3′	2193–2213
TaqMan probe	5′-CCAGTCCATTTGATTGGTTGTCACTTCCC-3′	2163–2191

oride membranes (Hybond®) by semidry electroblotting for 35 min. The blots were incubated with the purified antibody (1:4000 dilution) and detected on x-ray film by enhanced chemiluminescence with horseradish peroxidase-conjugated anti-rabbit IgG and cyclic diacylhydrazides (Amersham Biosciences). To confirm the specificity of the antibody, the antibody was absorbed with an excess amount of peptide (5 μg/ml) used as immunogen and processed similarly.

Real-time PCR—Real-time PCR was performed using the ABI PRISM 7700™ sequence detector (Applied Biosystems, Foster, CA) as described previously (21). The specific primers, the TaqMan probe, and the target sequence for real-time PCR are listed in Table II. The cDNA fragments of the target sequences were generated by RT-PCR with specific primers from rat kidney total RNA. Each PCR product was ligated into the pGEM-T-Easy vector (Promega, Madison, WI) and transformed into competent DH5α cells (Invitrogen). The concentrations of the purified plasmid DNA were measured by spectrophotometry, and corresponding copy numbers were calculated. Serial dilutions of the respective plasmid DNA were used as standards to make calibration curves. PCR amplification was performed in a total volume of 20 μl containing 5 μl of cDNA sample, 1 μM each primer, 0.2 μM TaqMan probe, and 10 μl of TaqMan Universal PCR Master Mix (Applied Biosystems). rGAPDH mRNA was also measured as an internal control with TaqMan® rodent GAPDH control reagents (Applied Biosystems).

Functional Expression and Uptake Analysis of rNaGLT1 in Xenopus oocytes—*Xenopus* oocytes were injected with water (50 nl) or rNaGLT1 cRNA (25 ng). Three days after injection, the uptake experiment was initiated by incubating oocytes at 25 °C in 500 μl of uptake buffer (96 mM NaCl, 2 mM KCl, 1.8 mM $CaCl_2$, 1 mM $MgCl_2$, and 5 mM HEPES, pH 7.4) containing α-[^{14}C]MeGlc or radiolabeled sugar analogs (37 kBq/ml) in the presence or absence of unlabeled inhibitors for 1 h unless otherwise indicated. Uptake in the absence of Na^+ or at a lowered Na^+ concentration was measured by substituting NaCl with choline chloride and by adding valinomycin. The uptake reaction was terminated by adding 2 ml of ice-cold uptake buffer, followed by washing the oocytes five times with 2 ml of the buffer. After the wash, each oocyte was dissolved with 300 μl of 10% SDS. Radioactivity was determined by adding 3 ml of ACSII (Amersham Biosciences) to each solubilized oocyte in a liquid scintillation counter.

Statistical Analysis—Data are expressed as means ± S.E. Data were analyzed statistically by one-way analysis of variance followed by Fisher's *t* test. Data from quantitative RT-PCR analysis were analyzed statistically using Student's paired *t* test with Bonferroni's correction.

RESULTS

A single cDNA clone encoding rNaGLT1 was isolated from the rat kidney cDNA library and sequenced. The rNaGLT1 cDNA consists of 2173 bp with an open reading frame encoding a 484-amino acid protein (calculated molecular mass of 51.7 kDa) and a poly(A)$^+$ tail. Fig. 1*A* shows the Kyte-Doolittle hydropathy analysis of rNaGLT1 (22). Membrane-spanning regions and the N-terminal orientation were predicted using the TMpred program (31)[2] and the SOSUI program (32).[3] On the basis of physicochemical properties (*i.e.* hydrophobicity,

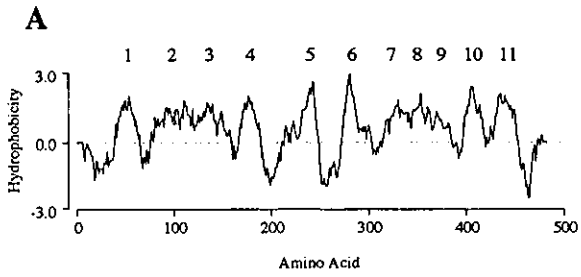

B

```
  1 MEFRGSGATAVEQHLLQSETPGKNGLQATSSDQVGRTLRWFTTVVLNAAFLGMGVSAAVL
                                                          M1
 61 GPTFPDLARNVNRNISSLSEIFVGRALGYLGGSVVGGVLFDCMNHFLLLGLSHLLTAAGL
                                    M2
121 YLTPFCKTAALLTAMMSITGVSFGVLDTGGNVLILDLWGDKGAPHIQALHFSFALGAFLA
                M3                                          M4
181 PLLAKLAWGTTASAQNHTEPQLDRSALNRSFEAASDSVLAVPDDMNLLWAYASIGTYVLV
                      *           *                         M5
241 LSVFLFAPFFKKRSKQKKSAASAQGARRAKYHRALLCLLFLFFFFYVGAEVTYGSYVFSF
                        ●                 M6
301 ATTHVGHEESEAAGLNSIFWGTFAACRGLAIFFATLLQPGTMMVLCNIGSLASSFFLVLF
                                M7                          M8
361 DKSPLCLWIASSVYGASMAATFPSGISWIEQYTTLTGKSAAFILVGAALGLMATPALSGI
                          M9                Δ               M10
421 LQGHYPDLPVILYMCLGSAVLTTVLFPVMYKVATLPLDRKQEKSINSEGQKILLSSSRLI
                          M11                                   Δ
481 KEAK
```

FIG. 1. **Hydropathy plot (*A*) and deduced amino acid sequence (*B*) of rNaGLT1.** *A*, shown is a Kyte-Doolittle hydropathy plot with a window of 13 amino acid residues. *Numbers* indicate putative membrane-spanning regions. *B*, potential *N*-linked glycosylation sites are indicated by *asterisks*. Potential protein kinase C (△) and protein kinase A (●) phosphorylation sites are indicated.

charges, and distribution) of amino acid residues and their sequences, an 11-transmembrane-spanning region model of rNaGLT1 was developed (Fig. 1*B*). The topology of rNaGLT1 includes five extracellular and five intracellular loops; the N terminus is oriented extracellularly; and the 34-amino acid C terminus is oriented toward the cytoplasm.

The amino acid sequence of rNaGLT1 shares <22% homology with known SGLT and GLUT glucose transporters and might belong to a new family of membrane transporters. Comparison of the amino acid sequence using the BLAST program revealed that rNaGLT1 shares a high degree of amino acid homology with three hypothetical proteins, of which only primary structures were clarified without any functional characterization (Table III). Compared with known proteins, rNaGLT1 is slightly homologous to the multidrug efflux transporter and the glucose/galactose transporter of *Xylella fastidiosa* in part (Table III). In addition, the rNaGLT1 amino

[2] Available at www.expasy.ch.
[3] Available at www.sosui.proteome.bio.taut.ac.jp.

TABLE III
Comparison of rNaGLT1 with hypothetical proteins
Homology was compared using GENETYX-MAC version 10.1. GenBank™/EBI accession numbers are given. AA, amino acids.

Gene name	Species	Length (AA)	Homology	Accession No.
			%	
Hypothetical protein XP 137057	Mouse	511	61	XM137057
Putative novel protein similar to bacterial nitrite extrusion protein	Mouse	366	62	BAB25402
Hypothetical protein XP 166307	Human	518	57	XP166307
Multidrug efflux transporter	*Bacillus halodurans*	409	22	NP242641
Glucose/galactose transporter	*X. fastidiosa*	426	24	NP298898

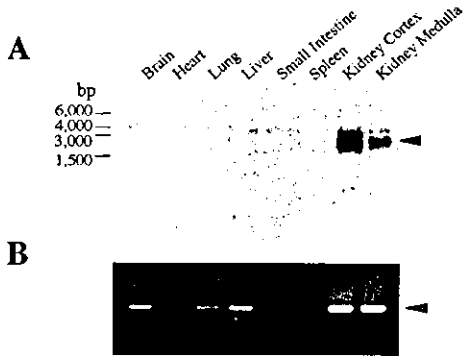

FIG. 2. **Northern blot analysis (*A*) and detection by PCR amplification (*B*) of rNaGLT1 mRNA in rat tissues.** *A*, poly(A)$^+$ RNA (1 μg) from the tissues indicated was electrophoresed, blotted, and hybridized with the specific probe for rNaGLT1 under high stringency conditions. *B*, poly(A)$^+$ RNA (1 μg) from the tissues indicated was reverse-transcribed, and the cDNA synthesized was amplified using a set of primers specific for rNaGLT1. The PCR products were separated by electrophoresis on 1% agarose gels and stained with ethidium bromide.

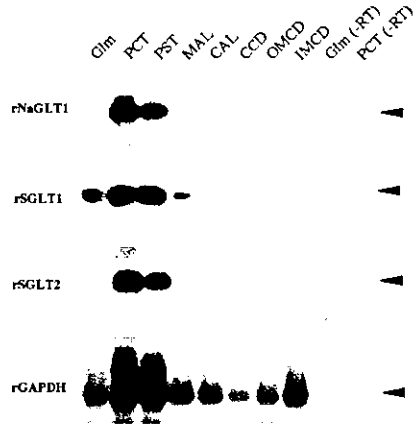

FIG. 3. **Detection of rNaGLT1, rSGLT1, and rSGLT2 mRNAs in microdissected renal nephron segments by RT-PCR and subsequent Southern blotting.** Each PCR amplification (35 cycles) was performed using part of the reverse transcription reaction derived from 20 glomeruli or 8 mm of renal tubule. The cDNA synthesized was amplified using a set of primers for rNaGLT1, rSGLT1, rSGLT2, and rGAPDH. The PCR products were separated by electrophoresis on 1.5% agarose gels. The agarose gels were transferred onto a nylon membrane and hybridized with the [^{32}P]dCTP-labeled rNaGLT1, rSGLT1, rSGLT2, and rGAPDH cDNAs as probes under high stringency conditions. *Glm*, glomerulus; *PCT*, proximal convoluted tubule; *PST*, proximal straight tubule; *MAL*, medullary thick ascending limb; *CAL*, cortical thick ascending limb; *CCD*, cortical collecting duct; *OMCD*, outer medullary collecting duct; *IMCD*, inner medullary collecting duct; *−RT*, without reverse transcriptase.

acid sequence does not contain any conserved domain when searched against the Smart[4] and Pfam[5] libraries.

We examined the tissue distribution of rNaGLT1 mRNA

[4] Available at smart.embl-heidelberg.de/.
[5] Available at pfam.wust1.edu/.

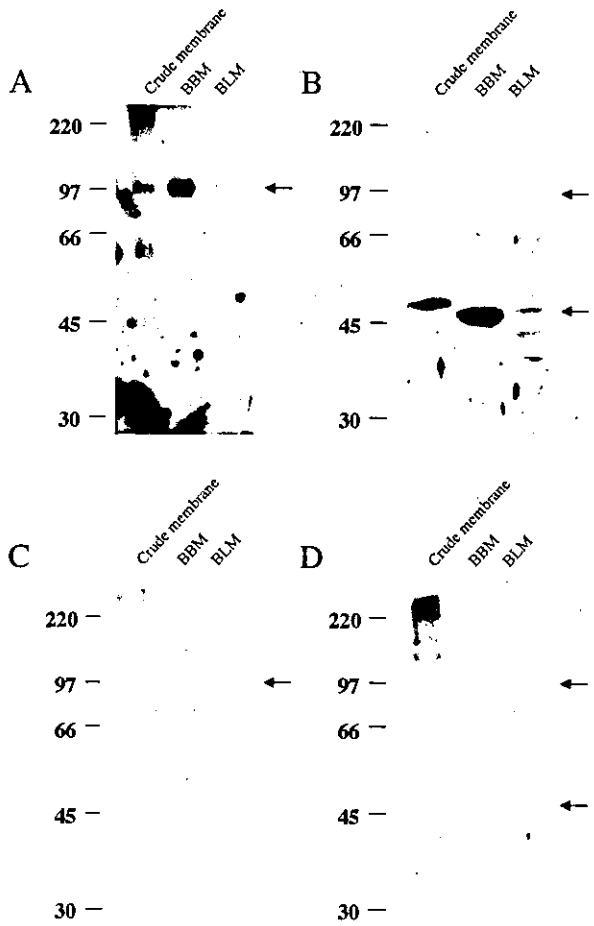

FIG. 4. **Immunoblot analysis of crude, brush-border, and basolateral membranes from rat kidney cortex with anti-rNaGLT1 antibody.** Forty micrograms of each membrane was separated by SDS-PAGE under nonreducing (*A* and *C*) or reducing (*B* and *D*) conditions. *A* and *B*, the affinity-purified antiserum for rNaGLT1 was used as the primary antibody. *C* and *D*, the affinity-purified antiserum preabsorbed with the antigen peptide (5 μg/ml) of rNaGLT1 was used. Horseradish peroxidase-conjugated anti-rabbit IgG was used for detection of bound antibodies, and the strips of blots were visualized by chemiluminescence on x-ray film. The *arrows* indicate the positions of 97 and 50 kDa. *BBM*, brush-border membrane; *BLM*, basolateral membrane.

transcripts by Northern blot analysis (Fig. 2*A*). Under high stringency conditions, a full-length rNaGLT1 probe was hybridized with mRNA transcripts from rat kidney cortex and medulla. For PCR analysis of rNaGLT1 mRNA expression, a set of specific primers for the cDNA of rNaGLT1 was used. As shown in Fig. 2*B*, a PCR product of the expected size for rNaGLT1 was found in rat brain, liver, lung, kidney cortex, and kidney medulla.

To examine the distribution of rNaGLT1 in the kidney, we performed RT-PCR analysis of the microdissected nephron segments. With RT and subsequent PCR and Southern blotting, a signal with the predicted size of 468 bp for rNaGLT1 was

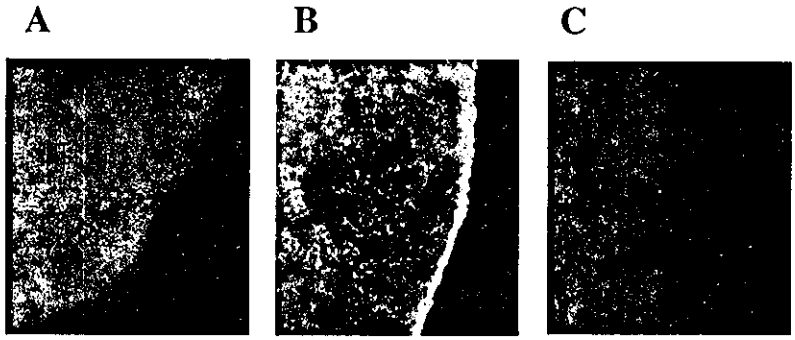

FIG. 5. **Expression of rNaGLT1 proteins in *Xenopus* oocytes.** Oocytes were injected with water (50 nl; *A*) or *in vitro* transcribed rNaGLT1 cRNA (25 ng/oocyte; *B* and *C*). Three days after injection, oocytes were fixed, frozen, sectioned, and stained as described under "Experimental Procedures." *A* and *B*, the affinity-purified antiserum for rNaGLT1 was used as the primary antibody. *C*, the affinity-purified antiserum preabsorbed with the antigen peptide (50 μg/ml) of rNaGLT1 was used. Cy3-labeled anti-rabbit IgG was used for detection of bound antibodies.

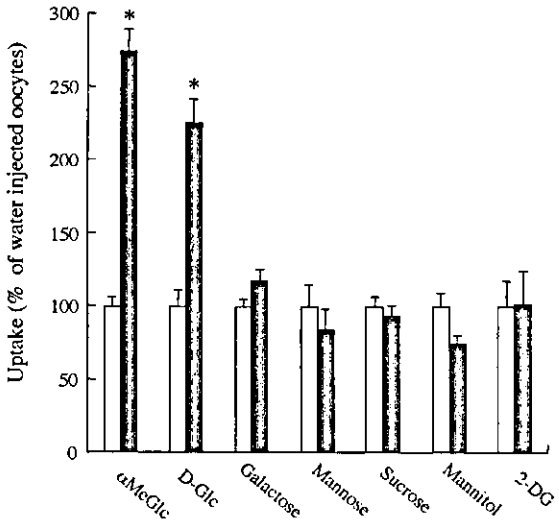

FIG. 6. **Uptake of sugar analogs by *Xenopus* oocytes injected with rNaGLT1 cRNA.** Uptake assays were performed with oocytes incubated at 25 °C for 1 h in buffer containing sugar analogs (2 mM, 37 kBq/ml) 3 days after injection of water (50 nl; *white bars*) or *in vitro* transcribed rNaGLT1 cRNA (25 ng/oocyte; *gray bars*). Each *bar* represents the mean ± S.E. of 8–10 oocytes. *, $p < 0.05$, significantly different from water-injected oocytes (Student's unpaired *t* test).

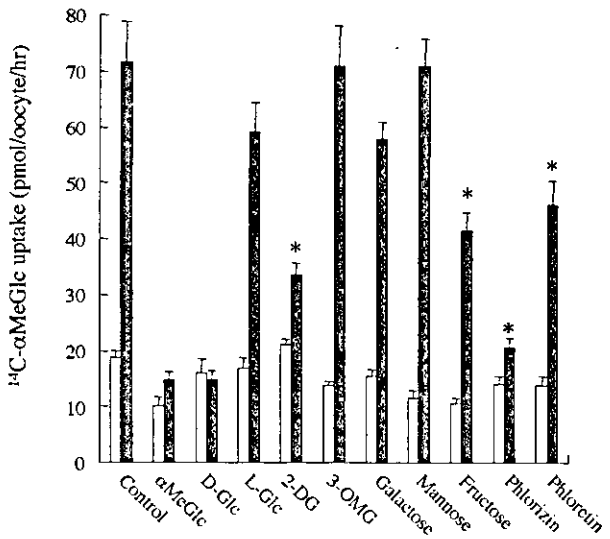

FIG. 7. **Effects of sugar analogs, phlorizin, and phloretin on α-[^{14}C]MeGlc uptake by *Xenopus* oocytes.** The uptake of α-MeGlc (2 mM, 37 kBq/ml) by oocytes was measured for 1 h at 25 °C in the absence and presence of sugar analogs (30 mM), phlorizin (50 μM), or phloretin (25 μM). *White bars*, oocytes injected with water (50 nl); *gray bars*, oocytes injected with *in vitro* transcribed rNaGLT1 cRNA (25 ng/oocyte). Each *bar* represents the mean ± S.E. of 8–10 oocytes. *, $p < 0.05$, significantly different from control values (Fisher's *t* test). *3-OMG*, 3-*O*-methylglucose.

detected in the proximal convoluted and straight tubules (Fig. 3). Faint signals with the same size were detected in the medullary thick ascending limb and cortical collecting duct. Similarly, rSGLT1 and rSGLT2 were also detected primarily in the proximal convoluted and straight tubules (Fig. 3).

To clarify the membrane localization of rNaGLT1 protein, we performed immunoblot analysis of rNaGLT1 in rat kidney crude membranes, brush-border membranes, and basolateral membranes using affinity-purified antibody against rNaGLT1. Under nonreducing conditions without dithiothreitol, an immunoreactive protein with an apparent molecular mass of 97 kDa was strongly expressed in the brush-border membrane fraction, slightly expressed in the crude membrane fraction, and faintly expressed in the basolateral membrane fraction (Fig. 4*A*). Under reducing conditions with 50 mM dithiothreitol, a signal was detected at ~50 kDa in the brush-border membrane fraction (Fig. 4*B*). The band in the crude membrane fraction was slightly larger than that in the brush-border membrane fraction. The immunoreactive bands in the brush-border and crude membranes were completely abolished when the antibody was preabsorbed with the antigen peptide (5 μg/ml) (Fig. 4, *C* and *D*), suggesting that the positive bands observed in the brush-border and crude membranes were specific for rNaGLT1. The oocytes expressing rNaGLT1 displayed strong signals along the plasma membranes and weak signals in the cytoplasm, although oocytes injected with water exhibited no labeling of the membranes or cytoplasm (Fig. 5, *A* and *B*). In addition, the signals were completely abolished when the antibody was preabsorbed with the antigen peptide (50 μg/ml) (Fig. 5*C*).

To characterize the transport function of rNaGLT1, the accumulation of various sugar analogs was measured in *Xenopus* oocytes injected with rNaGLT1 cRNA (Fig. 6). The uptake of α-MeGlc and D-glucose was significantly increased, but the other analogs tested showed little or no uptake in rNaGLT1 cRNA-injected compared with water-injected oocytes. The substrate specificity of rNaGLT1 was tested by inhibition experiments in which inhibition of the uptake of α-[^{14}C]MeGlc (2 mM for 1 h) was determined in the presence of various sugar analogs (30 mM), phlorizin (25 μM), or phloretin (50 μM) (Fig. 7). α-MeGlc, D-glucose, and phlorizin completely inhibited the uptake. The uptake of α-[^{14}C]MeGlc was strongly inhibited by 2-DG and slightly inhibited by fructose and phloretin, whereas L-glucose, 3-*O*-methylglucose, galactose, and mannose had little or no effect.

The saturation of α-MeGlc uptake in rNaGLT1-injected oocytes is demonstrated in Fig. 8*A*. Based on Eadie-Hofstee plot analysis, the apparent K_m and V_{max} values for α-MeGlc were calculated to be 3.71 ± 0.09 mM and 136.3 ± 17.0 pmol/oocyte/h, respectively. The Na^+ dependence of α-MeGlc uptake in rNaGLT1-injected oocytes was examined by measuring α-[^{14}C]MeGlc uptake as a function of extracellular [Na^+] with

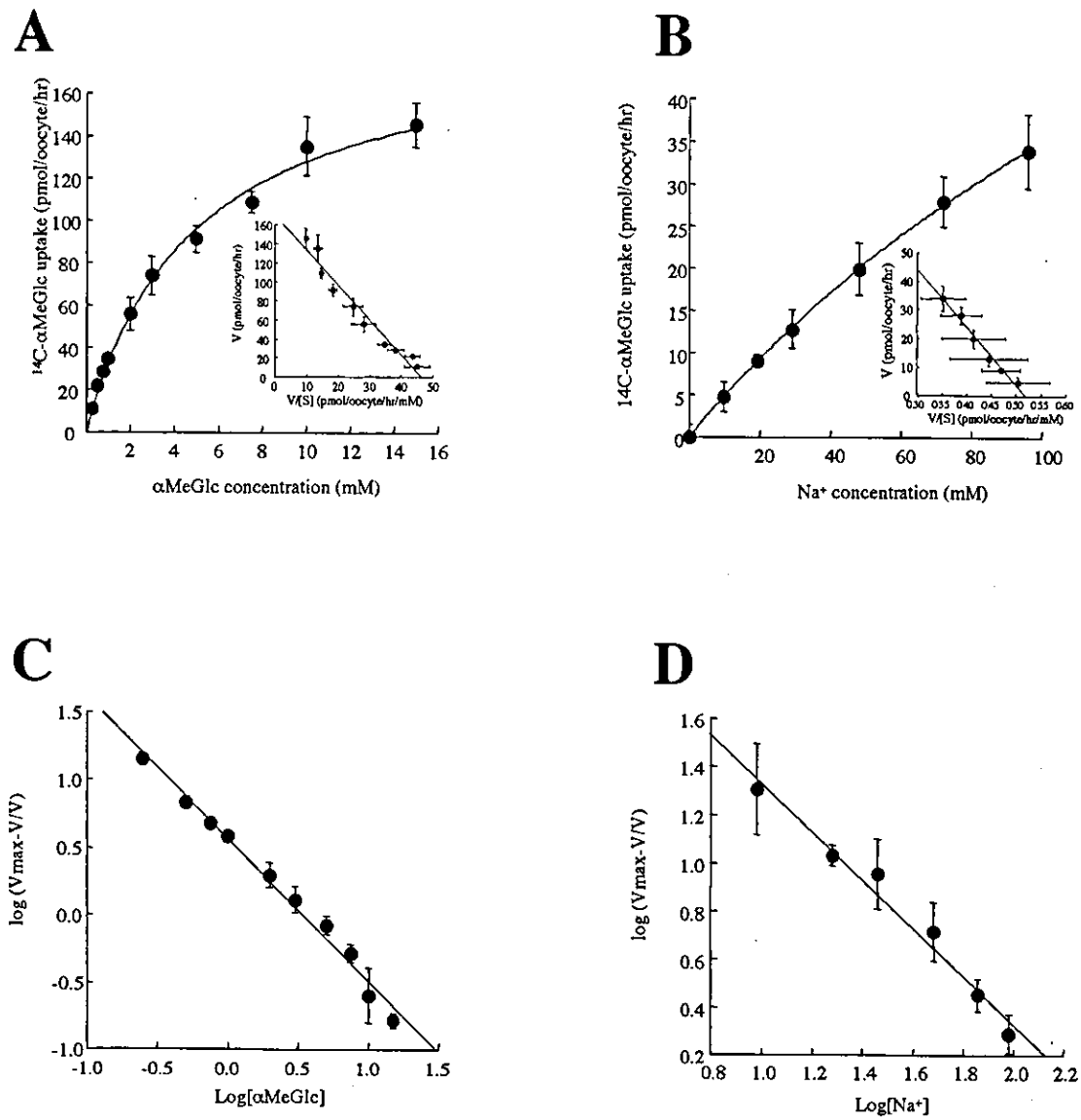

FIG. 8. **Concentration and Na^+ dependence of rNaGLT1-mediated α-MeGlc uptake by *Xenopus* oocytes.** *A*, the uptake of α-MeGlc by oocytes injected with rNaGLT1 cRNA (25 ng/oocyte) was assayed for 1 h at 25 °C in incubation buffer at various concentrations (0.5–15 mM), and the uptake measured in water-injected oocytes was subtracted. The *inset* shows an Eadie-Hofstee plot of the uptake. *B*, the uptake of α-MeGlc by oocytes injected with rNaGLT1 cRNA (25 ng/oocyte) was assayed for 1 h at 25 °C in incubation buffer at various Na^+ concentrations (0–96 mM), and the uptake measured in water-injected oocytes was subtracted. The *inset* shows an Eadie-Hofstee plot of the uptake. *C*, shown is a Hill (log to log) plot of the data from Fig. 8*A*. *D*, shown is a Hill plot of the data from Fig. 8*B*. Each point represents the mean ± S.E. of 8–10 oocytes. The apparent K_m values were obtained from three independent experiments.

the membrane voltage clamped to zero (equal internal and external $[K^+]$ in the presence of 7 μM valinomycin). In the rNaGLT1 cRNA-injected oocytes, the α-MeGlc uptake was stimulated by the extracellular Na^+ in a concentration-dependent manner, although the uptake was not saturated at Na^+ concentrations between 0 and 96 mM (Fig. 8*B*). Hill plot analyses using the data in Fig. 8 (*A* and *B*) gave coefficients of 1.06 and 1.00, respectively, indicating that the Na^+/glucose coupling ratio for rNaGLT1 is 1:1 (Fig. 8, *C* and *D*).

The results of Northern blotting of rNaGLT1, rSGLT1, and rSGLT2 in the kidney cortex or medulla are shown in Fig. 9. The relative quantity of rNaGLT1, rSGLT1, and rSGLT2 was estimated by densitometry. rNaGLT1 mRNA was expressed more abundantly in the cortex than in the medulla, and its expression level was higher than that of rSGLT1 or rSGLT2. To compare the expression levels of rNaGLT1 and rSGLT mRNAs precisely, we performed a quantitative RT-PCR analysis (Fig. 10). The mRNA levels of rNaGLT1 both in the cortex (Fig. 10*A*) and medulla (Fig. 10*B*) were significantly higher than those of rSGLT1 or rSGLT2.

DISCUSSION

We have isolated and characterized a cDNA encoding a novel Na^+-dependent glucose transporter (rNaGLT1) predominantly expressed in rat kidney. rNaGLT1 transports α-MeGlc in an Na^+-dependent manner with low substrate affinity, with the apparent K_m for α-MeGlc being 3.7 mM (Fig. 8). It is known that there are high and low affinity types of Na^+-dependent glucose transporters, whose K_m values are 0.35 and 6 mM, respectively, in rabbit kidney (23). rNaGLT1 was suggested to be one of the low affinity-type Na^+-dependent glucose transporters because the characteristics of rNaGLT1 are similar to those rSGLT2 in several ways, as follows: 1) its mRNA was abundantly expressed in the kidney cortex and primarily in the proximal convoluted and straight tubules (Figs. 2 and 3); 2) rNaGLT1 was expressed in the brush-border membranes of proximal

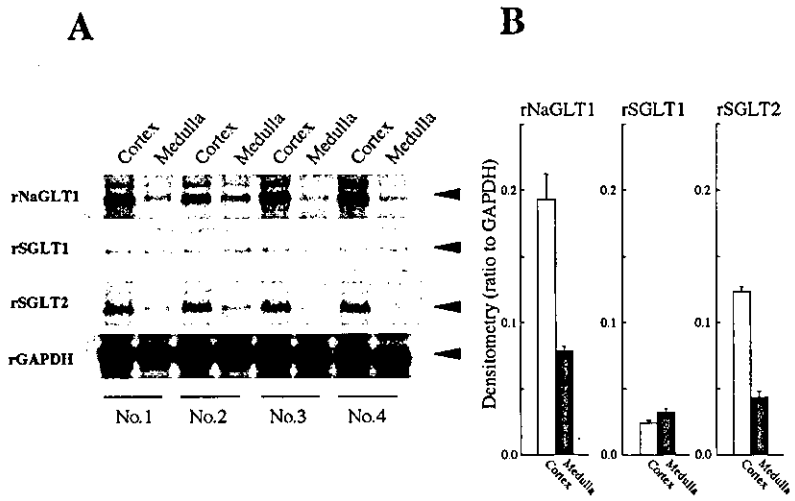

FIG. 9. **Northern blot analysis of rNaGLT1, rSGLT1, and rSGLT2 in the kidney cortex and medulla.** *A*, 5 μg of total RNA from the kidney cortices and medullas of four rats was electrophoresed, blotted, and hybridized with the probes for rNaGLT1, rSGLT1, rSGLT2, and rGAPDH under high stringency conditions. *B*, the amounts of mRNA were quantified by densitometry and normalized to rGAPDH. Each *bar* represents the mean ± S.E. of four rats.

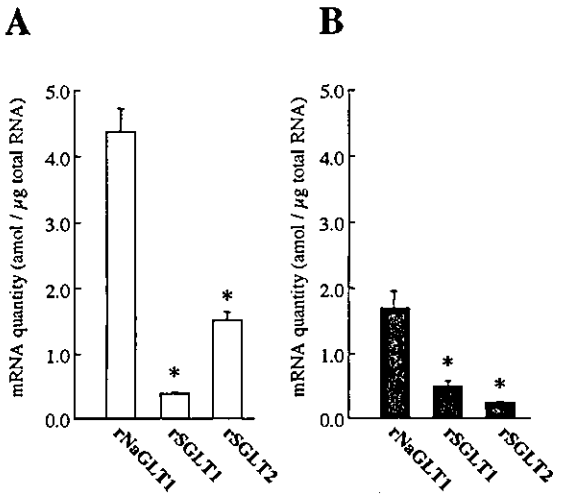

FIG. 10. **Quantification of rNaGLT1, rSGLT1, and rSGLT2 mRNAs in the kidney cortex (*A*) and medulla (*B*) by real-time PCR.** Total cellular RNA was extracted from rat kidney cortex (*A*) and medulla (*B*), and the extracted RNA was reverse-transcribed. The rNaGLT1, rSGLT1, and rSGLT2 mRNA levels were determined by real-time PCR using an ABI PRISM 7700™ sequence detector. Each *bar* represents the mean ± S.E. of four rats. *, $p < 0.05$, significantly different from rNaGLT1 (Student's paired *t* test with Bonferroni's correction).

tubules (Fig. 4); 3) galactose was not recognized as its substrate (Fig. 6); and 4) the coupling ratio of sodium to glucose was 1:1 (Fig. 8) (11). Despite such similarity to rSGLT2, rNaGLT1 shares a low degree of amino acid sequence homology with SGLTs or GLUTs. Our previous report demonstrated that the V_{max} for low affinity-type Na^+-dependent glucose transport activity in renal brush-border membrane vesicles was significantly decreased in the 5/6 nephrectomized rats, an animal model of chronic renal failure, compared with the sham-operated controls, although the expression level of SGLT2 mRNA was maintained in 5/6 nephrectomized rats (24). The reason for this discrepancy of low affinity-type glucose transport in the 5/6 nephrectomized rats remains unknown and could be accounted for by rNaGLT1. Therefore, rNaGLT1 would be another low affinity-type Na^+-dependent glucose transporter and belongs to a new gene family in view of its structure.

A signal corresponding to rNaGLT1 was recognized in the crude membrane fraction, and it was concentrated further in the brush-border membrane fraction by immunoblot analysis under nonreducing conditions (Fig. 4*A*). This indicates that rNaGLT1 was localized in the brush-border membranes of the proximal tubule. However, a faint band was also detected in the basolateral membrane fraction. The basolateral membrane fraction was purified by Percoll density gradient centrifugation (18). Although this method is useful for obtaining the basolateral membrane fraction, slight contamination of brush-border membranes cannot be avoided. Therefore, the faint band shown in the basolateral membrane fraction might be due to the contamination of brush-border membranes. The approximate molecular mass of the rNaGLT1 signal is 97 kDa (Fig. 4*A*). This is markedly larger than the molecular mass predicted from the amino acid sequence (51.7 kDa). However, when the crude and brush-border membrane fractions were reduced by dithiothreitol, a signal was detected at ~50 kDa, which is comparable to the predicted size of rNaGLT1 (Fig. 4*B*). These findings indicate that rNaGLT1 might form homodimer or a complex with other proteins.

rNaGLT1 mRNA was expressed abundantly in the kidney cortex (Fig. 2), and its level was ~3-fold higher in the cortex and 5-fold higher in the medulla compared with rSGLT2 mRNA (Fig. 10). Similar to rSGLT2, the uptake activity of α-[^{14}C]MeGlc in rNaGLT1 cRNA-injected oocytes is 2.5–4-fold higher than that in water-injected oocytes (11, 12). The low glucose uptake activity shown in rNaGLT1-expressing oocytes might be accounted for by the non-saturable extracellular concentration of Na^+, for which the apparent K_m was estimated as 202 mM, and/or by poor ability to express rNaGLT1.

The inhibitory effects of glucose analogs on the uptake of α-MeGlc in rNaGLT1-injected oocytes are almost comparable to those of rSGLT2, except for phloretin and 2-DG (Fig. 7) (11, 12). In general, phloretin and 2-DG are known to inhibit GLUT-mediated glucose transport (25, 26). However, phloretin slightly inhibits glucose transport in rat renal brush-border membrane vesicles (27). In addition, as the concentration of 2-DG (30 mM) induces ATP depletion and cytotoxicity (28), the inhibition of α-MeGlc uptake by 2-DG might be caused by a nonspecific disturbance of the activity. Taken together, the decrease in rNaGLT1-mediated uptake in the presence of phloretin and 2-DG is considered not to contradict previous findings of renal Na^+-dependent glucose transport.

The rNaGLT1 mRNA was detected only in the kidney cortex and medulla by Northern blot analysis (Fig. 2*A*). On the other hand, the amplified products corresponding to rNaGLT1 were detected not only in the kidney, but also in the brain, lung, and liver by RT-PCR analysis. rNaGLT1 mRNA was expressed primarily in the kidney, but rNaGLT1 itself or its homolog also might be expressed slightly in several other tissues. Previous reports showed that the brain and lung, as well as the intestine

and kidney, possess activity for Na^+-dependent glucose transport (29, 30). It remains to be clarified whether rNaGLT1 or its analog takes part in glucose transport in such tissues or not.

In this study, we successfully isolated rNaGLT1 from a rat kidney mRNA data base constructed by the random sequencing technique. This might be the first demonstration of the cloning of a novel transporter by the random sequencing of a cDNA library coupled with the functional expression technique. Although many genes have recently been submitted to public data bases such as the DDBJ/GenBank™/EMBL Data Bank, ~40% of the genes in the rat kidney data base are unknown. In addition, theoretically, a clone from the random sequence data base is expressed abundantly *in vivo* (6–8). Therefore, this method should be useful for the cloning of novel critical transporters. The physiological role of rNaGLT1, especially in correlation with SGLTs and GLUTs, remains to be clarified. Studies using diabetic and nephropathic animal models or gene knockout animals might be useful for the determination of the pathophysiological role of rNaGLT1.

REFERENCES

1. Collins, F. S., Patrinos, A., Jordan, E., Chakravarti, A., Gesteland, R., and Walters, L. (1998) *Science* **282,** 682–689
2. RIKEN Genome Exploration Research Group Phase II Team FANTOM Consortium (2001) *Nature* **409,** 685–690
3. Allikmets, R., Gerrard, B., Glavac, D., Ravnik-Glavac, M., Jenkins, N. A., Gilbert, D. J., Copeland, N. G., Modi, W., and Dean, M. (1995) *Mamm. Genome* **6,** 114–117
4. Phay, J. E., Hussain, H. B., and Moley, J. F. (2000) *Surgery* **128,** 946–951
5. Okubo, K., Hori, N., Matoba, R., Niiyama, T., Fukushima, A., Kojima, Y., and Matsubara, K. (1992) *Nat. Genet.* **2,** 173–179
6. Takenaka, M., Imai, E., Kaneko, T., Ito, T., Moriyama, T., Yamauchi, A., Hori, M., Kawamoto, S., and Okubo, K. (1998) *Kidney Int.* **53,** 562–572
7. Takenaka, M., Imai, E., Nagasawa, Y., Matsuoka, Y., Moriyama, T., Kaneko, T., Hori, M., Kawamoto, S., and Okubo, K. (2000) *Kidney Int.* **57,** 19–24
8. Nakajima, H., Takenaka, M., Kaimori, J., Nagasawa, Y., Kosugi, A., Kawamoto, S., Imai, E., Hori, M., and Okubo, K. (2002) *Kidney Int.* **61,** 1577–1587
9. Wright, E. M. (2001) *Am. J. Physiol.* **280,** F10–F18
10. Hediger, M. A., Coady, M. J., Ikeda, T. S., and Wright, E. M. (1987) *Nature* **330,** 379–381
11. You, G., Lee, W. S., Barros, E. J., Kanai, Y., Huo, T. L., Khawaja, S., Wells, R. G., Nigam, S. K., and Hediger, M. A. (1995) *J. Biol. Chem.* **270,** 29365–29371
12. Kanai, Y., Lee, W. S., You, G., Brown, D., and Hediger, M. A. (1994) *J. Clin. Invest.* **93,** 397–404
13. Turk, E., Zabel, B., Mundlos, S., Dyer, J., and Wright, E. M. (1991) *Nature* **350,** 354–356
14. Santer, R., Schneppenheim, R., Dombrowski, A., Gotze, H., Steinmann, B., and Schaub, J. (1997) *Nat. Genet.* **17,** 324–326
15. Saito, H., Masuda, S., and Inui, K.-i. (1996) *J. Biol. Chem.* **271,** 20719–20725
16. Masuda, S., Saito, H., Nonoguchi, H., Tomita K., and Inui, K.-i. (1997) *FEBS Lett.* **407,** 127–131
17. Uwai, Y., Okuda, M., Takami, K., Hashimoto, Y., and Inui, K.-i. (1998) *FEBS Lett.* **438,** 321–324
18. Ogihara, H., Saito, H., Shin, B. C., Terada, T., Takenoshita, S., Nagamichi, Y., Inui, K.-i., and Takata, K. (1996) *Biochem. Biophys. Res. Commun.* **220,** 848–852
19. Inui, K.-i., Okano, T., Takano, M., Kitazawa, S., and Hori, R. (1981) *Biochim. Biophys. Acta* **647,** 150–154
20. Takahashi, K., Nakamura, N., Terada, T., Okano, T., Futami, T., Saito, H., and Inui, K.-i. (1998) *J. Pharmacol. Exp. Ther.* **286,** 1037–1042
21. Motohashi, H., Sakurai, Y., Saito, H., Masuda, S., Urakami, Y., Goto, M., Fukatsu, A, Ogawa, O, and Inui, K.-i. (2002) *J. Am. Soc. Nephrol.* **13,** 866–874
22. Kyte, J., and Doolittle, R. F. (1982) *J. Mol. Biol.* **157,** 105–132
23. Turner, R. J., and Moran, A. (1982) *Am. J. Physiol.* **242,** F406–F414
24. Takahashi, K., Masuda, S., Nakamura, N., Saito, H., Futami, T., Doi, T., and Inui, K.-i. (2001) *Am. J. Physiol.* **281,** F1109–F1116
25. Cheung, P. T., and Hammerman, M. R. (1988) *Am. J. Physiol.* **254,** F711–F718
26. Rumsey, S. C., Kwon, O., Xu, G. W., Burant, C. F., Simpson, I., and Levine, M. (1997) *J. Biol. Chem.* **272,** 18982–18989
27. Kinne, R., Murer, H., Kinne-Saffran, E., Thees, M., and Sachs, G. (1975) *J. Membr. Biol.* **21,** 375–395
28. Sridhar, R., Stroude, E. C., and Inch, W. R. (1979) *In Vitro (Rockville)* **15,** 685–690
29. Lee, W. J., Peterson, D. R., Sukowski, E. J., and Hawkins, R. A. (1997) *Am. J. Physiol.* **272,** C1552–C1557
30. Oelberg, D. G., Xu, F., and Shabarek, F. (1994) *Biochim. Biophys. Acta* **1194,** 92–98
31. Hoffmann, K., and Stoffel, W. (1993) *Biol. Chem.* **374,** 166
32. Hirokawa, T., Boon-Chieng, S., and Mitaku, S. (1998) *Bioinformatics* **14,** 378–379

FEBS Letters 546 (2003) 276–280 FEBS 27375

Na^+-dependent fructose transport via rNaGLT1 in rat kidney

Naoshi Horiba, Satohiro Masuda, Chiharu Ohnishi, Daisuke Takeuchi, Masahiro Okuda, Ken-ichi Inui*

Department of Pharmacy, Kyoto University Hospital, Faculty of Medicine, Kyoto University, Sakyo-ku, Kyoto 606-8507, Japan

Received 22 April 2003; revised 16 May 2003; accepted 17 May 2003

First published online 2 June 2003

Edited by Stuart Ferguson

Abstract We found a system of Na^+-dependent uptake of fructose by rat renal brush-border membrane vesicles. It consisted of two saturable components, and was thought to involve at least two transporters. rNaGLT1, a novel glucose transporter in rat kidney, showed fructose uptake as well as α-methyl-D-glucopyranoside uptake by transfected HEK293 cells. The features of the lower affinity type of fructose transporter in the brush-border membranes, such as affinity and substrate recognition, were very comparable with those of rNaGLT1-transfected HEK293 cells. These results indicated that rNaGLT1 is a primary fructose transporter in rat renal brush-border membranes.

Key words: Rat Na^+-dependent glucose transporter 1; Fructose; Kidney; Brush-border membrane vesicle; Na^+-dependent

1. Introduction

Fructose is found as a free monosaccharide and in combination with various other sugars and complex carbohydrates. Unlike glucose, which is absorbed across the small intestine by SGLT1, fructose uptake occurs via the sodium-independent facilitative transporters GLUT5 and GLUT2 [1–4]. In the small intestine, GLUT5 is present in the brush-border membranes and it is proposed that the transepithelial transport of dietary fructose involves apical entry via GLUT5 and subsequent basolateral exit via GLUT2 [5]. Several findings have been reported about fructose uptake in the small intestine, such as regulation or genetic polymorphisms, but renal reabsorption or excretion of fructose has remained to be elucidated [6–8]. Although GLUT5 has been thought to play a primary role in renal fructose reabsorption in the brush-border membranes, it is localized only in the S3 segment, not in the S1 and S2 segments, of renal proximal tubules [9]. Because the basolateral fructose transporter GLUT2 is localized only in S1 and S2 and not in S3 of proximal tubules, the role of these transporters in the transepithelial transport of fructose remains unclear [9,10].

Recently, we have identified an Na^+-dependent glucose transporter (rNaGLT1) in rat kidney [11]. rNaGLT1 cRNA-injected oocytes transport α-methyl-D-glucopyranoside (αMeGlc) and D-glucose in an Na^+-dependent manner. rNaGLT1 mRNA is abundantly expressed in the kidney cortex, primarily in the proximal convoluted tubules. rNaGLT1 protein is expressed in the brush-border membranes of proximal tubules and is thought to reabsorb glucose from the lumen to tubular cell. Considering its localization along the nephron, affinity for glucose transport and recognition of substrates, rNaGLT1 was suggested to be a low affinity type of glucose transporter similar to SGLT2, a sodium-dependent glucose transporter [11,12]. But rNaGLT1 showed less than 22% homology in amino acid sequence with known glucose transporters, SGLTs and GLUTs, and its precise role, especially in terms of the difference from SGLT2, remains unknown. In the present study, we found an Na^+-dependent uptake system for fructose using rat renal brush-border membrane vesicles, and rNaGLT1 was suggested to be a candidate for a low affinity type transporter.

2. Materials and methods

2.1. Materials

D-[U-^{14}C]Fructose (9.18 GBq/mmol) and [1,2-^{3}H]2-deoxy-D-glucose (2-DG) (925 GBq/mmol) were purchased from Moravek Biochemicals (Brea, CA, USA). [U-^{14}C]αMeGlc (11.7 GBq/mmol) was obtained from Amersham Biosciences (Uppsala, Sweden). Unlabeled D-fructose, αMeGlc, D-galactose, 3-*O*-methylglucose and D-sucrose were purchased from Nacalai Tesque (Kyoto, Japan). Phlorizin, phloretin and 2-DG were obtained from Sigma (St. Louis, MO, USA). 2,5-Anhydromannitol was from Toronto Research Chemicals (North York, ON, Canada). All other chemicals were of the highest purity available.

2.2. Cell culture and transfection

HEK293 cells (American Type Culture Collection CRL-1573), a transformed cell line derived from human embryonic kidney, were cultured in complete medium consisting of Dulbecco's modified Eagle's medium (Sigma) with 10% fetal calf serum (Whittaker Bioproducts, Walkersville, MD, USA) in an atmosphere of 5% CO_2, 95% air at 37°C. pBK-CMV plasmid vector containing rNaGLT1 cDNA was purified using the Marligen High Purity Plasmid Purification Midiprep System (Marligen Bioscience, Ijamsville, MD, USA). The day before the transfection, HEK293 cells were seeded onto poly-D-lysine-coated 24-well plates at a density of 2.0×10^5 cells/well. The cells were transfected with 0.8 μg of total plasmid DNA per well using LipofectAMINE 2000 (Invitrogen Life Technologies, Carlsbad, CA, USA) according to the manufacturer's instructions. At 48 h after transfection, the cells were used for uptake experiments.

2.3. Uptake experiment in HEK293 cells

Cellular uptake of [^{14}C]fructose was measured with monolayer cultures grown on poly-D-lysine-coated 24-well plates. The composition of the incubation medium was as follows: 145 mM NaCl, 3 mM KCl, 1 mM $CaCl_2$, 0.5 mM $MgCl_2$ and 5 mM 4-(2-hydroxyethyl)-1-piperazineethanesulfonic acid (HEPES) (pH 7.4). Uptake in the absence of Na^+ was measured by substituting NaCl with choline chloride. The

*Corresponding author. Fax: (81)-75-751 4207.
E-mail address: inui@kuhp.kyoto-u.ac.jp (K.-i. Inui).

Abbreviations: rNaGLT1, rat Na^+-dependent glucose transporter 1; αMeGlc, α-methyl-D-glucopyranoside; 2-DG, 2-deoxy-D-glucose

0014-5793/03/$22.00 © 2003 Published by Elsevier Science B.V. on behalf of the Federation of European Biochemical Societies.
doi:10.1016/S0014-5793(03)00600-8

cells were preincubated with 0.2 ml of incubation medium for 15 min at 37°C. The medium was then removed, and 0.2 ml of incubation medium containing [^{14}C]fructose, [^{14}C]αMeGlc or [^{3}H]2-DG was added. The medium was aspirated at the end of the incubation period, and the monolayers were rapidly washed twice with 1 ml of ice-cold incubation medium. The cells were solubilized in 0.5 ml of 0.5 N NaOH, and then the radioactivity in aliquots was determined by liquid scintillation counting. The protein content of the solubilized cells was determined by the method of Bradford [13] using a Bio-Rad Protein Assay Kit (Bio-Rad Laboratories, Hercules, CA, USA) with bovine γ-globulin as a standard.

2.4. Preparation of renal brush-border membrane vesicles

The renal brush-border membranes were isolated from the renal cortex of 7-week-old male rats by the Mg^{2+}/EGTA precipitation method as described previously [14]. The isolated membranes were suspended in an experimental buffer to give a final protein concentration of 7–8 mg/ml. In general, the final experimental buffer consisted of either 100 mM mannitol, 100 mM NaCl or KCl and 10 mM HEPES (pH 7.5), and the pH was adjusted with tris(hydroxymethyl) aminomethane. Uptake in the absence of Na^+ was measured by substituting NaCl with choline chloride.

2.5. Uptake analysis in renal brush-border membrane vesicles

The uptake of [^{14}C]fructose by brush-border membrane vesicles was measured by a rapid filtration technique as described previously [14]. Usually, membrane vesicles suspended in an appropriate buffer were preincubated for 10 min at 25°C before the initiation of uptake. The uptake was initiated by the addition of 20 μl of a buffer containing 4 mM [^{14}C]fructose (final 2 mM) to 20 μl of membrane suspension at 25°C. At the specified periods, the incubation was terminated by diluting the reaction mixture with 1 ml of ice-cold stop solution containing 150 mM NaCl, 20 mM HEPES-Tris (pH 7.5) and 0.1 mM phlorizin. The mixture was poured immediately onto Millipore filters (HAWP, 0.45 μm, 2.5 cm diameter), and the filters were washed with 5 ml of ice-cold stop solution. The radioactivity of the [^{14}C]fructose trapped in membrane vesicles was determined in ACS II (Amersham Biosciences) by liquid scintillation counting.

2.6. Statistical analysis

Data are expressed as the mean ± S.E.M. and were analyzed statistically using Student's unpaired *t*-test. For multiple comparisons, data were analyzed statistically by one-way analysis of variance followed by Fisher's *t*-test.

3. Results

3.1. rNaGLT1 mediated fructose uptake by HEK293 cells

To characterize the transport function of rNaGLT1, the accumulation of fructose, αMeGlc and 2-DG, a substrate specific for facilitative glucose transporters, was measured with rNaGLT1-transfected HEK293 cells. The reproducible uptake of fructose was significantly increased as was that of αMeGlc, but 2-DG showed little or no uptake by rNaGLT1-transfected HEK293 cells compared with vector-transfected cells (Fig. 1A).

We measured the initial uptake of fructose by rNaGLT1-transfected HEK293 cells in the presence of Na^+, varying the concentration of fructose (0.1–20 mM). The saturation of fructose uptake by rNaGLT1-transfected HEK293 cells is demonstrated in Fig. 1B. Based on Eadie–Hofstee plot analysis, the apparent K_m and V_{max} values for fructose were calculated to be 4.55 ± 0.29 mM and 311.5 ± 38.5 pmol/mg protein/min, respectively. The uptake of D-glucose by rNaGLT1-transfected cells could not be measured owing to high activity of endogenous transporters.

3.2. Na^+-dependent uptake of fructose by renal brush-border membrane vesicles

To analyze whether the uptake of fructose in renal brush-border membranes was Na^+-dependent or -independent, brush-border membrane vesicles from rat kidney were incubated in the presence of 100 mM NaCl or KCl. In the presence of an inward Na^+ gradient, fructose uptake was apparently accelerated, with the initial uptake at 15 s four-fold higher than in the absence of an Na^+ gradient (Fig. 2A).

The initial uptake rate for fructose (15 s) was examined as a function of the fructose concentration. The specificity of the

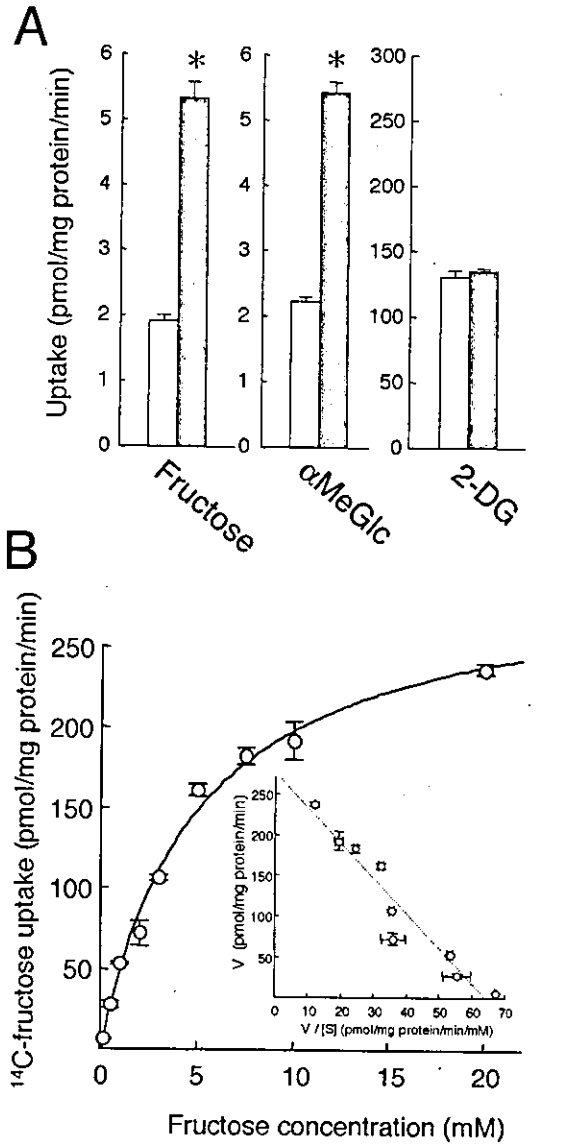

Fig. 1. rNaGLT1 mediated fructose uptake by HEK293 cells. A: Uptake assays were performed with HEK293 cells incubated at 37°C for 15 min with the buffer containing sugar analogues (0.1 mM, 37 kBq/ml) 2 days after transfection of vector (open column, 0.8 μg/well) or rNaGLT1 cDNA (closed column, 0.8 μg/well). Each column represents the mean ± S.E.M. of three monolayers. *$P < 0.05$, significantly different from vector-transfected HEK293 cells (Student's unpaired *t*-test). B: Uptake of [^{14}C]fructose by HEK293 cells transfected with rNaGLT1 cDNA (0.8 μg/well) was assayed for 15 min at 37°C in incubation buffer at various concentrations (0.1–20 mM) and the uptake measured in the vector-transfected HEK293 cells was subtracted. Inset shows an Eadie–Hofstee plot of the uptake. Each point represents the mean ± S.E.M. of three monolayers. The apparent K_m and V_{max} values were obtained from three separate experiments.

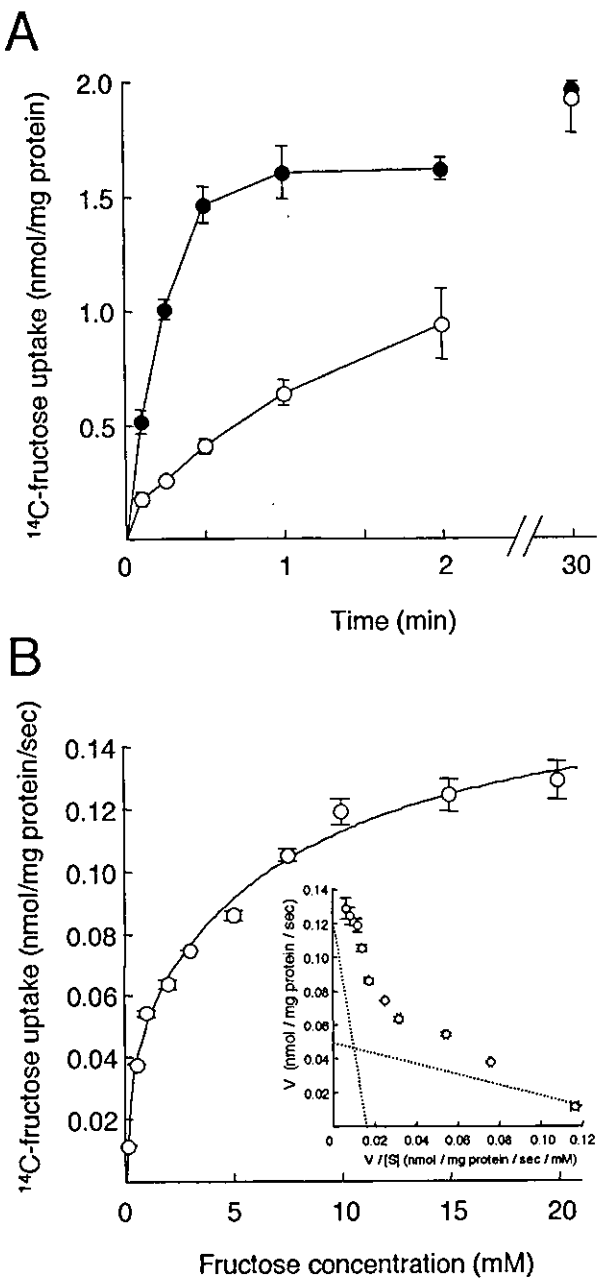

Fig. 2. Uptake of fructose by renal brush-border membrane vesicles. A: Membrane vesicles (20 μl) suspended in 100 mM mannitol and 10 mM HEPES (pH 7.5) were incubated at 25°C with a substrate mixture (20 μl) comprising 100 mM mannitol, 200 mM NaCl (closed circles) or KCl (open circles), 4 mM [^{14}C]fructose and 10 mM HEPES (pH 7.5). Each value represents the mean ± S.E.M. of three separate experiments. Each experiment was performed using the brush-border membrane vesicles isolated from five rats. B: Na^+-dependent uptake of fructose by renal brush-border membrane vesicles was assayed for 15 s at 25°C in incubation buffer at various concentrations (0.1–20 mM) in the presence of NaCl, and the uptake substituting NaCl with KCl was subtracted. Inset shows an Eadie–Hofstee plot of the uptake. Each point represents the mean ± S.E.M. of three determinations. The apparent K_m and V_{max} values were obtained from three separate experiments.

Na^+-dependent fructose uptake was calculated by subtracting the uptake in the presence of KCl from that in the presence of NaCl. Fig. 2B shows the Na^+-dependent fructose uptake concentration dependence curve. Eadie–Hofstee plot analysis indicated that the Na^+-dependent uptake consisted of two saturable components. The kinetic parameters of this uptake were calculated using a non-linear least squares regression analysis with two Michaelis–Menten equations for two transport systems. The K_m and V_{max} values for the higher affinity type of fructose uptake were 0.29 ± 0.04 mM and 30.1 ± 4.9 pmol/mg protein/s, respectively. Those for the lower affinity type were 7.84 ± 0.12 mM and 102.1 ± 14.9 pmol/mg protein/s, respectively.

3.3. *Characteristics of Na^+-dependent fructose transport in rNaGLT1-transfected HEK293 cells and renal brush-border membranes*

The substrate specificities of rNaGLT1-transfected HEK293 cells and renal brush-border membrane vesicles were tested by inhibition experiments, in which the inhibition of the uptake of [^{14}C]fructose (HEK293 cells, 0.1 mM for 15 min; brush-border membrane vesicles, 2 mM for 15 s) was determined in the presence and absence of either sugar analogues (30 mM), phlorizin (50 μM) or phloretin (50 μM) (Table 1). The uptake of [^{14}C]fructose was strongly inhibited by fructose, αMeGlc, phlorizin and the lack of an Na^+ gradient, whereas little or no inhibitory effect was exerted by sucrose and 3-*O*-methylglucose both in the rNaGLT1-transfected HEK293 cells and in the brush-border membranes. Galactose little affected the uptake by rNaGLT1-transfected HEK293 cells but slightly inhibited the uptake by renal brush-border membrane vesicles. 2,5-Anhydromannitol, an inhibitor of GLUT5 [15], and phloretin strongly inhibited the uptake by the rNaGLT1-transfected HEK293 cells, but only slightly inhibited the uptake by the brush-border membrane vesicles. 2-DG strongly inhibited the uptake by the brush-border membrane vesicles, but slightly inhibited the uptake by the rNaGLT1-transfected HEK293 cells.

4. Discussion

Fructose as well as glucose is absorbed in the small intestine and renal proximal tubules. In the basolateral membrane, fructose was transported in an Na^+-independent manner via GLUT2 [4]. The Na^+-dependence of fructose uptake by the brush-border membrane vesicles from the small intestine has remained controversial. Sigrist-Nelson and Hopfer [16], Guy and Deren [17], and Honegger and Semenza [18] reported that mucosal flux of fructose was unaffected by Na^+. In contrast, Bihler [19], Gracey et al. [20], and Macrae and Neudoerffer [21] reported an Na^+-dependent fructose transport in the small intestine. GLUT5, isolated from human small intestine, is localized to the brush-border membranes of small intestine and renal proximal tubules [2,3,22]. The expression level of GLUT5 protein, which was regulated by dietary fructose, corresponded well to the level of fructose absorption in vivo and GLUT5 is thought to be one of the major fructose transporters of the brush-border membranes in the small intestine [23]. However, the findings that fructose malabsorption disease did not result from the expression of mutant GLUT5 protein and that the stimulation of fructose absorption by sucrose was not explained by GLUT5 suggest the existence of an alternative fructose transporter in addition to GLUT5 [7,23]. Recently, we isolated rNaGLT1, a novel Na^+-dependent glucose transporter, from rat kidney [11]. In the present study, fructose as well as αMeGlc was transported by rNaGLT1 in an Na^+-

Table 1
Effects of sugar analogues, phlorizin and phloretin on [^{14}C]fructose uptake by rNaGLT1-transfected HEK293 cells or renal brush-border membrane vesicles

Addition	rNaGLT1-mediated [^{14}C]fructose uptake by HEK293 cells		Na^+-dependent [^{14}C]fructose uptake by renal brush-border membranes	
	pmol/mg protein/min	% of control	pmol/mg protein/s	% of control
Control	2.92 ± 0.04	100	49.5 ± 3.6	100
Absence of Na^+	0.16 ± 0.20*	5	−0.2 ± 1.3*	0
Fructose	0.22 ± 0.06*	8	5.4 ± 2.1*	11
αMeGlc	1.24 ± 0.13*	42	23.8 ± 2.1*	48
Galactose	2.88 ± 0.23	99	35.2 ± 3.3	71
3-OMG	2.60 ± 0.15	89	47.1 ± 4.5	95
2-DG	2.04 ± 0.19*	70	16.8 ± 3.7*	34
Sucrose	4.20 ± 0.17*	144	47.3 ± 6.0	96
2,5-AM	1.16 ± 0.16*	40	38.6 ± 2.6	78
Phlorizin	0.34 ± 0.11*	12	3.2 ± 0.8*	6
Phloretin	0.97 ± 0.09*	33	35.8 ± 3.5	72

[^{14}C]Fructose (0.1 mM, 37 kBq/ml) uptake by rNaGLT1-transfected HEK293 cells was measured for 15 min at 37°C in the absence and presence of either sugar analogues (30 mM), phlorizin (50 μM) or phloretin (50 μM), and the uptake measured in the vector-transfected HEK293 cells was subtracted. Membrane vesicles (20 μl) suspended in 100 mM mannitol and 10 mM HEPES (pH 7.5) were incubated for 15 s at 25°C with a substrate mixture (20 μl) comprising [^{14}C]fructose (final 2 mM, 74 kBq/ml) in the absence and presence of either sugar analogues (30 mM), phlorizin (50 μM) or phloretin (50 μM), and the uptake substituting NaCl with KCl was subtracted. The absence of Na^+ was the uptake measured in the condition substituting NaCl with choline chloride. Each value represents the mean ± S.E.M. of three separate experiments. *$P < 0.05$, significantly different from control values (Fisher's t-test). 3-OMG, 3-O-methylglucose; 2,5-AM, 2,5-anhydromannitol.

dependent manner (Fig. 1A, Table 1). Unlike in the small intestine, there have been few reports about fructose reabsorption by renal proximal tubules. We report here for the first time the Na^+-dependent fructose uptake by renal brush-border membrane vesicles consisting of two saturable components whose apparent K_m values were 0.3 and 7.8 mM, respectively (Fig. 2B). As the apparent K_m value for rNaGLT1-mediated fructose uptake was 4.5 mM (Fig. 1B), rNaGLT1 was suggested to be the low affinity type of fructose transporter in renal brush-border membranes.

The effects of sugar analogues and phlorizin on the uptake of fructose by renal brush-border membrane vesicles were very comparable with those by rNaGLT1-transfected HEK293 cells. We previously found that the mRNA expression level of rNaGLT1 in the kidney was higher than that of SGLTs [11]. These results indicated that rNaGLT1 plays a crucial role in the Na^+-dependent fructose uptake in renal brush-border membranes. Although the effects of galactose, phloretin, 2,5-anhydromannitol and 2-DG on the uptake of fructose by renal brush-border membrane vesicles were not in total agreement with that of rNaGLT1-transfected HEK293 cells, the differences might be due to the high affinity type of fructose transporter in renal brush-border membranes or endogenous transporter(s).

GLUT5 localizes in the S3 segment of proximal tubules in the rat kidney, but its role in the transepithelial transport of fructose remains elusive [9,10]. Mate et al. [24] reported that fructose was transported in an Na^+-independent manner in the brush-border membranes of rat kidney and GLUT5 took part in the process. However, there have been no other reports about whether renal reabsorption of fructose is Na^+-dependent or not, and the involvement of GLUT5. In addition, Na^+-independent fructose uptake by renal brush-border membranes was non-saturable up to 50 mM, and its apparent K_m value was found to be more than 50 mM (data not shown). In this study, we found that renal fructose uptake was apparently Na^+-dependent. The reason for the discrepancy between the present data and the previous report remains unknown. However, in proximal convoluted tubules, rNaGLT1 was localized in the brush-border membranes but GLUT2 in the basolateral membranes and the K_m value of Na^+-dependent fructose uptake was considerably lower than that of Na^+-independent uptake. Taken together, rNaGLT1 was suggested to play an important role in the renal reabsorption of fructose at the proximal tubules.

In summary, we found Na^+-dependent fructose uptake in rat renal brush-border membranes. The features of the low affinity type of Na^+-dependent fructose uptake by renal brush-border membrane vesicles were very comparable with those by rNaGLT1-expressing HEK293 cells. Therefore, rNaGLT1 would be responsible for renal fructose reabsorption.

Acknowledgements: This work was supported by a Grant-in-Aid for Research on Human Genome, Tissue Engineering, and Food Biotechnology H12-Genome-019 from the Ministry of Health, Labor, and Welfare of Japan and by a Grant-in-Aid for Scientific Research from the Ministry of Education, Culture, Sports, Science, and Technology of Japan.

References

[1] Hediger, M.A., Coady, M.J., Ikeda, T.S. and Wright, E.M. (1987) Nature 330, 379–381.
[2] Burant, C.F., Takeda, J., Brot-Laroche, E., Bell, G.I. and Davidson, N.O. (1992) J. Biol. Chem. 267, 14523–14526.
[3] Rand, E.B., Depaoli, A.M., Davidson, N.O., Bell, G.I. and Burant, C.F. (1993) Am. J. Physiol. 264, G1169–G1176.
[4] Cheeseman, C.I. (1993) Gastroenterology 105, 1050–1056.
[5] Thorens, B. (1996) Am. J. Physiol. 270, G541–G553.
[6] Fujisawa, T., Riby, J. and Kretchmer, N. (1991) Gastroenterology 101, 360–367.
[7] Wasserman, D., Hoekstra, J.H., Tolia, V., Taylor, C.J., Kirschner, B.S., Takeda, J., Bell, G.I., Taub, R. and Rand, E.B. (1996) J. Clin. Invest. 98, 2398–2402.
[8] Solberg, D.H. and Diamond, J.M. (1987) Am. J. Physiol. 252, G574–G584.
[9] Sugawara-Yokoo, M., Suzuki, T., Matsuzaki, T., Naruse, T. and Takata, K. (1999) Kidney Int. 56, 1022–1028.
[10] Thorens, B., Lodish, H.F. and Brown, D. (1990) Am. J. Physiol. 259, C286–C294.
[11] Horiba, N., Masuda, S., Takeuchi, A., Takeuchi, D., Okuda, M. and Inui, K. (2003) J. Biol. Chem. 278, 14669–14676.

[12] You, G., Lee, W.S., Barros, E.J., Kanai, Y., Huo, T.L., Khawaja, S., Wells, R.G., Nigam, S.K. and Hediger, M.A. (1995) J. Biol. Chem. 270, 29365–29371.
[13] Bradford, M.M. (1976) Anal. Biochem. 72, 248–254.
[14] Takahashi, K., Masuda, S., Nakamura, N., Saito, H., Futami, T., Doi, T. and Inui, K. (2001) Am. J. Physiol. 281, F1109–F1116.
[15] Kane, S., Seatter, M.J. and Gould, G.W. (1997) Biochem. Biophys. Res. Commun. 238, 503–505.
[16] Sigrist-Nelson, K. and Hopfer, U. (1974) Biochim. Biophys. Acta 367, 247–254.
[17] Guy, M.J. and Deren, J.J. (1971) Am. J. Physiol. 221, 1051–1056.
[18] Honegger, P. and Semenza, G. (1973) Biochim. Biophys. Acta 318, 390–410.
[19] Bihler, I. (1969) Biochim. Biophys. Acta 183, 169–181.
[20] Gracy, M., Burke, V. and Oshin, A. (1972) Biochim. Biophys. Acta 266, 397–406.
[21] Macrae, A.R. and Neudoerffer, T.S. (1972) Biochim. Biophys. Acta 288, 137–144.
[22] Kayano, T., Burant, C.F., Fukumoto, H., Gould, G.W., Fan, Y.S., Eddy, R.L., Byers, M.G., Shows, T.B., Seino, S. and Bell, G.I. (1990) J. Biol. Chem. 265, 13276–13282.
[23] Burant, C.F. and Saxena, M. (1994) Am. J. Physiol. 267, G71–G79.
[24] Mate, A., de la Hermosa, M.A., Barfull, A., Planas, J.M. and Vazquez, C.M. (2001) Cell. Mol. Life Sci. 58, 1961–1967.

0022-3565/03/3072-626–632$7.00
THE JOURNAL OF PHARMACOLOGY AND EXPERIMENTAL THERAPEUTICS

JPET 307:626–632, 2003

Vol. 307, No. 2
55939/1103689
Printed in U.S.A.

Altered Diurnal Rhythm of Intestinal Peptide Transporter by Fasting and Its Effects on the Pharmacokinetics of Ceftibuten

XIAOYUE PAN, TOMOHIRO TERADA, MASAHIRO OKUDA, and KEN-ICHI INUI

Department of Pharmacy, Kyoto University Hospital, Faculty of Medicine, Kyoto University, Kyoto, Japan

Received June 19, 2003; accepted July 30, 2003

ABSTRACT

We previously demonstrated that H^+/peptide cotransporter PEPT1 shows a diurnal rhythm in the rat small intestine. In the present study, we examined the effect of food intake on the diurnal rhythm of intestinal PEPT1 using fed and fasted rats and also determined whether such variation affected the pharmacokinetics of peptide-like drugs. In fed rats, PEPT1 protein level was significantly higher at 8:00 PM than at 8:00 AM. However, during fasting for 2 to 4 days, the differences of PEPT1 protein levels between 8:00 AM and 8:00 PM gradually disappeared. Intestinal absorption of an oral antibiotic ceftibuten (CETB), a pharmacological substrate for PEPT1, was also greater at 8:00 PM than at 8:00 AM in fed rats, but not different in 4-day fasted rats. In contrast to PEPT1 protein levels, PEPT1 mRNA levels retained a diurnal rhythm after 4 days of fasting. Pharmacokinetic analyses of CETB after intraintestinal administration demonstrated that both C_{max} and area under the plasma concentration-time curve from 0 to 3 h were greater at 8:00 PM than at 8:00 AM in fed rats. In contrast, pharmacokinetic parameters showed no significant difference between 8:00 AM and 8:00 PM for intraintestinal administration in 4-day fasted rats and for intravenous administration in fed and 4-day fasted rats. These findings suggested that the diurnal rhythm of intestinal PEPT1 transport activity was disrupted by fasting and that diurnal variation of intestinal PEPT1 functionality could influence the pharmacokinetics of peptide-like drugs such as CETB.

Di- and tripeptides and various peptide-like drugs such as β-lactam antibiotics are taken up into the intestinal and renal epithelial cells by H^+-coupled peptide cotransporters. Cloning studies have identified two peptide transporters, PEPT1 and PEPT2, and many functional studies using heterologous expression systems have demonstrated molecular natures in their transport characteristics (Leibach and Ganapathy, 1996; Daniel and Herget, 1997; Inui and Terada, 1999). Furthermore, molecular identification of PEPT1 and PEPT2 provided a novel opportunity to determine the mechanisms of their regulation. For example, it was reported that the intestinal PEPT1 is regulated by various factors, including dietary conditions (Ogihara et al., 1999; Shiraga et al., 1999; Naruhashi et al., 2002), hormones such as insulin, leptin, and thyroid hormone (Buyse et al., 2001; Ashida et al., 2002; Gangopadhyay et al., 2002), epidermal growth factor (Nielsen et al., 2001), development (Shen et al., 2001), and some pharmacological agents (Fujita et al., 1999; Berlioz et al., 2000).

In addition to the above-described regulations, we recently found that PEPT1 in the rat small intestine is under the regulation of diurnal rhythm (Pan et al., 2002). Briefly, the transport of [^{14}C]glycylsarcosine (Gly-Sar), a typical substrate for PEPT1, by in situ intestinal loop and everted intestine was greater in the dark phase rather than the light phase, and PEPT1 protein and mRNA levels varied significantly, with a maximum at 8:00 PM and minimum at 8:00 AM (Pan et al., 2002). In contrast to the intestine, renal PEPT1 and PEPT2 showed little diurnal rhythmicity. Because rodents show nocturnal feeding behavior, the diurnal rhythm of intestinal PEPT1 is reasonable for the preparation of anticipated dietary load.

In our previous study, we used rats kept with free access to water and laboratory chow to clarify the diurnal rhythmicity under standard environmental conditions. However, because feeding conditions greatly affected the expression and function of intestinal PEPT1 (Ogihara et al., 1999; Shiraga et al., 1999; Naruhashi et al., 2002), there is a possibility that feeding also influences the diurnal rhythm of this transporter. Based on these hypotheses, in the present study, we examined the effect of food intake on the diurnal rhythm of intestinal PEPT1 using fed and fasted rats. In addition, using an oral β-lactam antibiotic ceftibuten (CETB), a good pharmacological substrate of PEPT1, we examined whether the regulation of intestinal PEPT1 in the diurnal rhythm and fasting could affect the intestinal absorption and pharmaco-

This work was supported in part by a Grant-in-Aid for Scientific Research from the Ministry of Education, Culture, Sports, Science and Technology of Japan.
Article, publication date, and citation information can be found at http://jpet.aspetjournals.org.
DOI: 10.1124/jpet.103.055939.

ABBREVIATIONS: PEPT, peptide transporter; CETB, ceftibuten; HPLC, high-performance liquid chromatography; AUC, area under the plasma concentration-time curve.

kinetics of this drug. The expressional changes of renal PEPT1 and PEPT2 were also examined to clarify the tissue specificity of the diurnal rhythm and fasting effect.

Materials and Methods

Materials. CETB was supplied by Shionogi Co. (Osaka, Japan). All other chemicals used were of the highest purity available.

Animals. Male Wistar rats (160–180 g) were housed in an air-conditioned room at 22 ± 0.5°C with a 12-h lighting schedule (8:00 AM–8:00 PM). Animals were fed ad libitum on the light/dark schedule for 1 week before they were divided into fed and fasted groups. Two different groups of rats were used in this study: 1) control group fed normal chow ad libitum (F0); and 2) fasted for 1 to 4 days (F1, F2, F3, and F4). Water was available ad libitum to all groups throughout the experiments. Five or six rats were used in each group. Daily changes in body and mucosal weights were examined over the 4 days of fasting (27 and 35% decreased in body and mucosal weights after 4 days of fasting, respectively, compared with those in fed rats). The animal experiments were performed in accordance with the Guidelines for Animal Experiments of Kyoto University.

Western Blot Analysis. Under anesthesia, the duodenum and kidney were removed at 8:00 AM and 8:00 PM of 1 day. The duodenum was flushed with ice-cold phosphate-buffered saline, and the mucosa was scraped. The kidney was decapsulated, and slices of the renal cortex were prepared with a Stadie-Riggs microtome. A portion of the mucosa and renal slices were rapidly frozen in liquid nitrogen for later preparation of brush-border membranes and total RNA. Brush-border membranes from rat small intestine and kidney cortex were prepared as described previously (Inui et al., 1984; Okano et al., 1986). The membrane fractions (small intestine, 10 μg/lane; kidney cortex, 50 μg/lane) were separated by 8.5% SDS-polyacrylamide gel electrophoresis, and analyzed by Western blot analyses as reported previously (Saito et al., 1995 and 1996). The relative densities of the bands in each reaction were determined using NIH Image 1.61 (National Institutes of Health, Bethesda, MD).

Northern Blot Analysis. Total RNA was isolated from small intestinal mucosa using TRIzol reagents (1 ml/100 mg of tissue) (Invitrogen Japan KK, Tokyo, Japan) per the manufacturer's protocols. Total RNA (20 μg/lane) was electrophoresed in 1% denaturing agarose gel containing formaldehyde, and Northern blot analyses were performed as reported previously (Saito et al., 1995, 1996; Pan et al., 2002).

In Situ Loop Technique. CETB absorption was examined by the in situ loop technique at 8:00 AM and at 8:00 PM in fed or 4-day fasted rats as described previously (Pan et al., 2002). The CETB (3 mg/3 ml/kg b.wt.) was introduced into a duodenum 10-cm loop with a microsyringe, and blood was withdrawn from the portal vein at 0, 3, 6, 9, 12, 15, 18, and 30 min after CETB injection. The blood samples were centrifuged for 2 min at 14,000*g*, and 100 μl of plasma samples were analyzed by high-performance liquid chromatography (HPLC).

In Vivo Experiments. Rats were anesthetized with sodium pentobarbital (40 mg/kg). For intraintestinal infusion of CETB, a catheter with a 26-gauge needle was carefully fixed with cyanoacrylate glue into the middle part of the duodenum (Yamaguchi et al., 2002). For intravenous infusion of CETB, the jugular vein was cannulated with a polyethylene-10 tube (BD Biosciences, Parsippany, NJ). A single 3 mg/kg body weight dose of CETB dissolved in an isotonic phosphate buffer (pH 6.0) was administered by the intraintestinal or the intravenous to fed and 4-day fasted rats at 8:00 AM or 8:00 PM. Blood samples were collected from the contralateral jugular vein at 0, 8, 15, 30, 45, and 60 min, and 1.5, 2.0, 2.5, and 3.0 h after CETB injection. The blood samples were centrifuged for 2 min at 14,000*g*, and 100 μl of plasma samples was analyzed by HPLC.

Pharmacokinetic Analysis. A conventional one-compartment model was used to analyze the plasma concentration-time profiles of CETB after intravenous administration in rats. Estimated pharmacokinetic parameters were total area under the plasma concentration-time curve from 0 h to 3 h area under the curve ($AUC_{0-3\ h}$) (linear trapezoidal method), maximum plasma concentration (C_{max}), time after administration needed to obtain C_{max} (T_{max}), elimination rate constant (K_e), half-life ($t_{1/2}$), volume of distribution (V_d), and total body clearance (CL_{tot}) for CETB.

HPLC Analysis. Plasma concentration of CETB was measured with an HPLC LC-6A (Shimadzu, Kyoto, Japan) equipped with an UV spectrophotometric detector SPD-10A (Shimadzu). The condition was as follows: column, Zorbax ODS 4.6-mm inside diameter × 150 mm (Agilent, Palo Alto, CA); mobile phase, 50 mM ammonium acetate/methanol (80:20); flow rate, 1.0 ml/min; wavelength, 262 nm; injection volume, 50 μl, and column temperature, 45°C. Peak area size was measured with a Chromatopac C-R6A (Shimadzu).

Data Analysis. Values are expressed as means ± S.E. Analysis of variance and Fisher's test were used for the statistical significance of CETB concentration and CETB pharmacokinetic parameters. The statistical significance of differences between mean values of other data was analyzed using the nonpaired *t* test or one-way analysis of variance followed by Fisher's test when multiple comparisons were needed. Differences were considered significant at $p < 0.05$.

Results

In our previous study, we found that PEPT1 protein and mRNA expressions were minimum at 8:00 AM (beginning of the light phase) and maximum at 8:00 PM (beginning of the dark phase), respectively (Pan et al., 2002), and thus we typically examined PEPT1 expression levels at these times. Furthermore, in preliminary experiments, the body weight and small intestinal mucosal mass of rats fasted for 1 to 4 days were significantly lower than those of fed rats. There was no significant difference in the loss of body weight or intestinal mucosal mass between at 8:00 AM and at 8:00 PM of each day. This result served to confirm the change of the intestinal mucosa during the fasting process.

Effect of Fasting on Diurnal Variation of Intestinal PEPT1 Protein and mRNA Levels in Fasted Rats. It has been demonstrated that starvation markedly increased the amount of intestinal PEPT1 mRNA (Naruhashi et al., 2002) and protein (Ogihara et al., 1999). In addition, in the present experiments, PEPT1 mRNA and protein levels in 4-day fasted rats were significantly increased compared with those in fed rats, and this effect was observed at both 8:00 AM and 8:00 PM (Fig. 1).

Next, we assessed diurnal regulation of intestinal PEPT1 protein using 1- to 4-day fasted rats. As shown in Fig. 2, in fed (F0) and the 1-day fasted rats (F1), PEPT1 protein level was significantly higher at 8:00 PM than at 8:00 AM. However, after fasting for 2 to 4 days (F2–F4), the differences of PEPT1 protein levels between 8:00 AM and 8:00 PM gradually disappeared. To exclude the possibility of the phase shift for intestinal PEPT1 biorhythm, we examined PEPT1 protein levels at 4-h intervals in 4-day fasted rats. As shown in Fig. 3, the intestinal PEPT1 protein of 4-day fasted rats showed no significant diurnal rhythm throughout 1 day.

To assess whether abolished diurnal variation of intestinal PEPT1 protein in 4-day fasted rats were transcriptionally regulated, Northern blot analysis was performed. As shown in Fig. 4, PEPT1 mRNA levels at 8:00 PM were significantly higher in 4-day fasted rats as well as in fed rats. These findings suggested that diurnal regulation of PEPT1 mRNA expression was maintained in the fasting state.

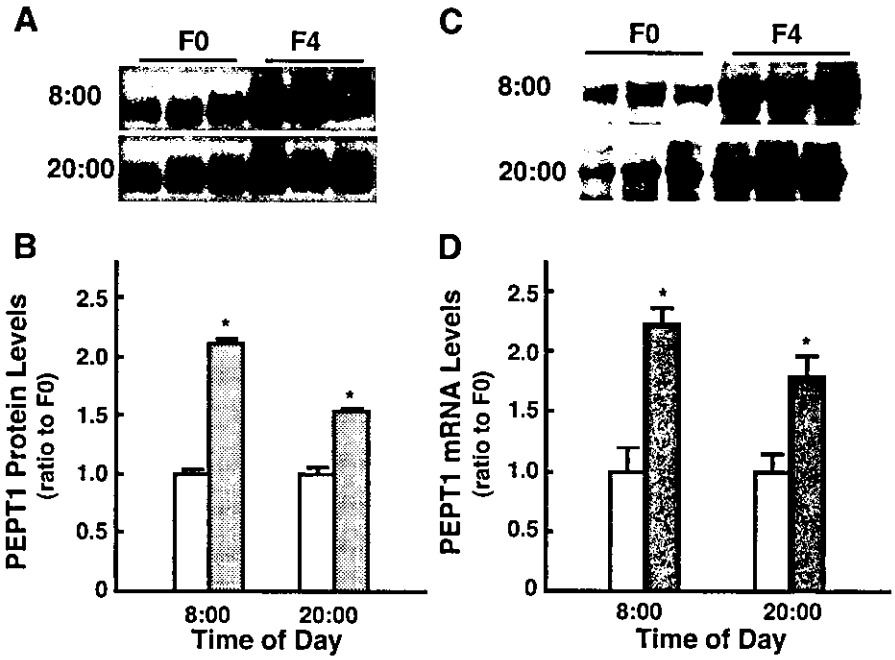

Fig. 1. Effect of fasting on PEPT1 protein (A and B) and mRNA (C and D) expression in the rat duodenum. A and B, duodenal brush-border membranes were prepared from fed (□) and 4-day fasted (■) rats killed at 8:00 AM and at 8:00 PM, and Western blot analyses were carried out. Representative data are shown in A. C and D, total RNA prepared from fed (□) and 4-day fasted (■) rats killed at 8:00 AM and at 8:00 PM, and Northern blot analyses were performed. Representative data are shown in C. Signal intensities on the film were subjected to scanning densitometry, and protein and mRNA abundances were expressed as a ratio of the value of fed rats. Each column represents the mean ± S.E. of five to six rats. *, $p < 0.05$, significantly different from fed rats.

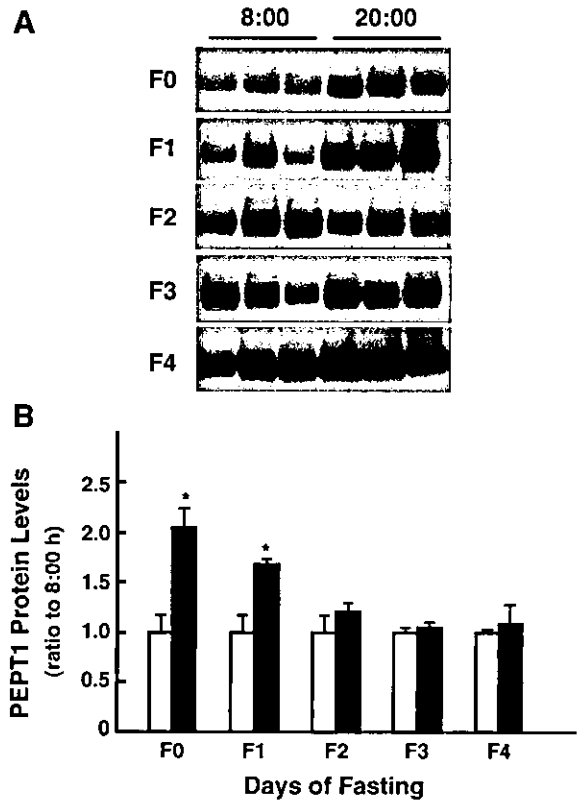

Fig. 2. Effect of fasting on diurnal variation of duodenal PEPT1 protein expression in the fed and fasted rats. A, duodenal brush-border membranes were prepared from fed and each fasted condition rats killed at 8:00 AM and at 8:00 PM, and Western blot analyses were carried out. Representative data are shown. B, signal intensities on the film were subjected to scanning densitometry, and protein abundances were expressed as a ratio of the value at 8:00 AM (□, 8:00 AM; ■, 8:00 PM). Each column represents the mean ± S.E. of five to six rats. *, $p < 0.05$, significantly different from 8:00 AM.

Effect of Fasting on Diurnal Variation of Renal PEPT1 and PEPT2 Protein Levels in Fasted Rats. We next examined the effect of fasting on renal PEPT1 and PEPT2 protein levels at 8:00 AM and 8:00 PM in fed and 4-day fasted rats. As shown in Fig. 5A, PEPT1 protein levels remained mostly constant between fed and 4-day fasted rats both at 8:00 AM and 8:00 PM. PEPT2 protein levels showed a similar pattern as PEPT1, but a modest decrease was observed at 8:00 AM (Fig. 5B).

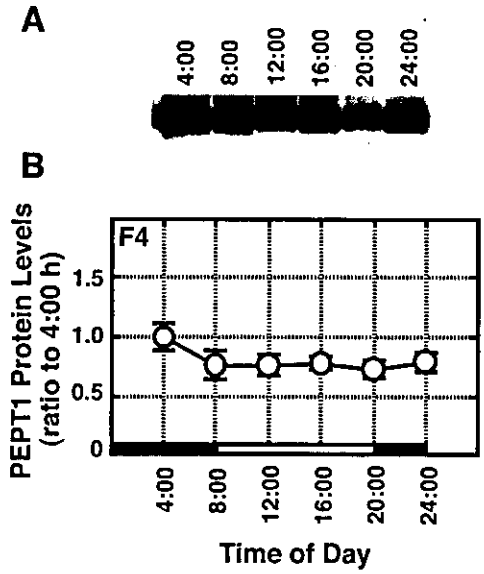

Fig. 3. Effect of fasting on duodenal PEPT1 protein expression in the 4-day fasted rats through 1 day. A, duodenal brush-border membranes were prepared from rats killed at the indicated time through 1 day, and Western blot analyses were carried out. Representative data are shown. B, signal intensities on the film were subjected to scanning densitometry, and protein abundances were expressed as a ratio of the value at 4:00 AM. □ and ■ show light and dark phases, respectively. Each point represents the mean ± S.E. of four rats.

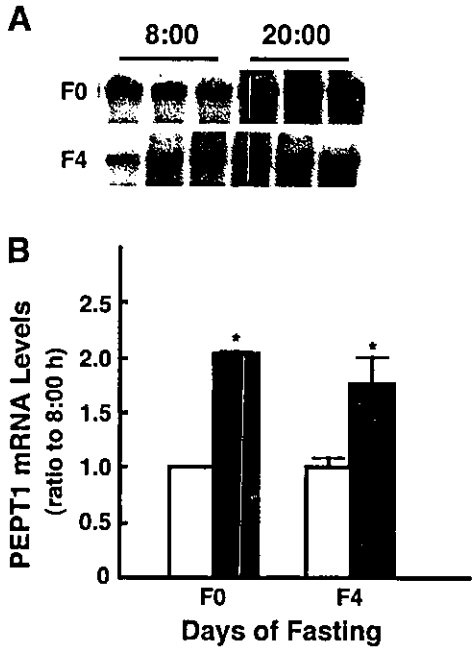

Fig. 4. Diurnal variation of duodenal PEPT1 mRNA expression in the fed and 4-day fasted rats. A, total RNA prepared from duodenum of fed and 4-day fasted rats killed at 8:00 AM and at 8:00 PM, and Northern blot analyses were performed. Representative data are shown. B, PEPT1 message levels were quantified by scanning densitometry, and expressed as a ratio of the value at 8:00 AM (□, 8:00 AM; ■, 8:00 PM). Each column represents the mean ± S.E. of five rats. *, $p < 0.05$, significantly different from at 8:00 AM.

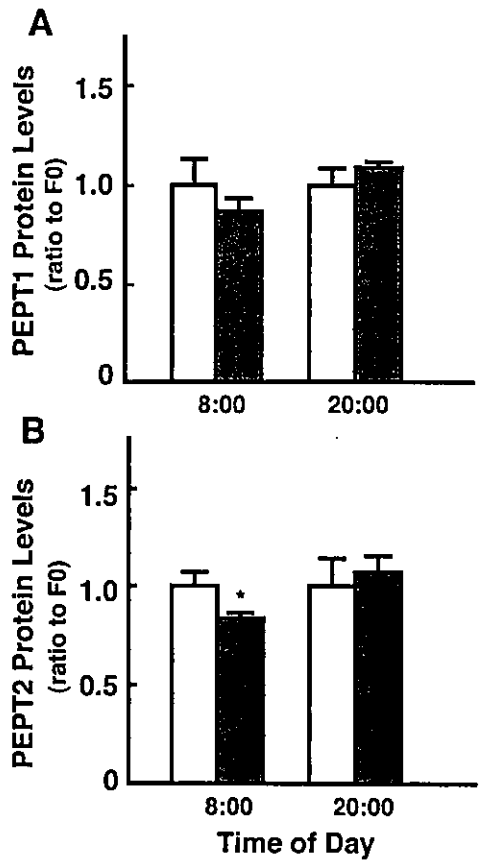

Fig. 5. Effect of fasting on renal PEPT1 (A) and PEPT2 (B) protein expression in fed and fasted rats. Brush-border membranes of rat kidney cortex were prepared from fed (□) and fasted (■) rats killed at 8:00 AM and 8:00 PM, and Western blot analyses were carried out. Signal intensities on the film were subjected to scanning densitometry, and protein abundances were expressed as a ratio of the value of fed rats. Each column represents the mean ± S.E. of six rats. *, $p < 0.05$, significantly different from at 8:00 AM.

Renal PEPT1 and PEPT2 did not show diurnal variation in the fed rats (Pan et al., 2002). This result was confirmed in the present study, as shown in F0 of Fig. 6, A and B. However, as the fasting period was prolonged, renal PEPT1 and PEPT2 protein levels showed a slight diurnal variation, with higher expression levels at 8:00 PM than at 8:00 AM in 4-day fasted rats (Fig. 6, A and B), suggesting distinct regulation of renal peptide transporters from that of the intestine.

CETB Pharmacokinetics at 8:00 AM and 8:00 PM in Fed and 4-Day Fasted Rats. It has been demonstrated that several drugs vary in potency and/or toxicity based on the rhythmicity of biochemical, physiological, and behavioral processes (Lemmer and Labrecque, 1987; Labrecque and Bélanger, 1991; Lemmer, 1999). There is a possibility that the diurnal regulation of intestinal PEPT1 may affect the intestinal absorption of peptide-like drugs, which in turn may influence the pharmacokinetic parameters of such drugs. Thus, we assessed this hypothesis using a representative pharmacological PEPT1 substrate CETB. Fasting effects on the intestinal absorption and the pharmacokinetic parameters of CETB were also investigated. As shown in Fig. 7, in the fed state, the initial absorption rate of CETB was significantly higher at 8:00 PM than at 8:00 AM. On the other hand, in the 4-day fasted state, the initial absorption rate of CETB was not significantly different between 8:00 AM and 8:00 PM. Comparing the initial absorption rate of CETB between fed and fasted rats, the latter showed higher absorption rate.

We next measured plasma concentrations of CETB after intraintestinal and intravenous administration at 8:00 AM and 8:00 PM in fed and 4-day fasted rats. Pharmacokinetic parameters of CETB after intraintestinal and intravenous administration are summarized in Tables 1 and 2, respectively. In the fed condition, rats administered at 8:00 AM showed greater C_{max} and $AUC_{0-3\ h}$, and faster T_{max} rather than those administered at 8:00 AM (Table 1; Fig. 8A). However, there were no significant differences of pharmacokinetic parameters of CETB between 8:00 AM and 8:00 PM in 4-day fasted rats (Table 1; Fig. 8B). Comparison of pharmacokinetic parameters between fed and 4-day fasted rats, all parameters exhibited higher absorption of CETB in 4-day fasted rats compared with fed rats irrespective of administration time (Table 1). In the intravenous administration, there were no differences in K_e, CL_{tot}, and $t_{1/2}$ between 8:00 AM and 8:00 PM in the fed and 4-day fasted rats (Table 2; Fig. 8, C and D), although there were significant differences between fed and 4-day fasted rats at both administration times (Table 2).

Discussion

A daily periodicity in the intestinal transport activity and several other digestive proteins were documented before the responsible genes were identified. Nevertheless, the observed activity changes were clearly ascribed to the feeding pattern (ad libitum and scheduled) rather than to an inherent circadian signal (Fisher and Gardner, 1976; Stevenson and Fi-

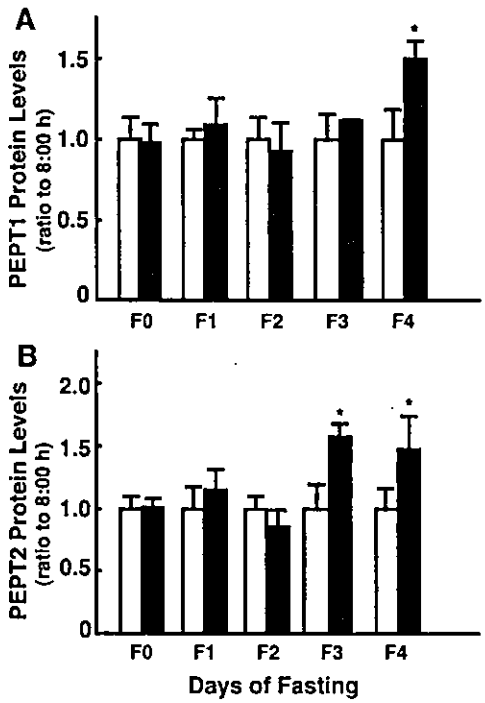

Fig. 6. Diurnal variation of renal PEPT1 (A) and PEPT2 (B) protein expression in the fed and fasted rats. Renal brush-border membranes were prepared from fed and each fasted condition rats killed at 8:00 AM and at 8:00 PM of 1 day, and Western blot analyses were carried out. Signal intensities on the film were subjected to scanning densitometry, and protein abundances were expressed as a ratio of the value at 8:00 AM (□, 8:00 AM; ■, 8:00 PM). Each column represents the mean ± S.E. of six rats. *, $p < 0.05$, significantly different from at 8:00 AM.

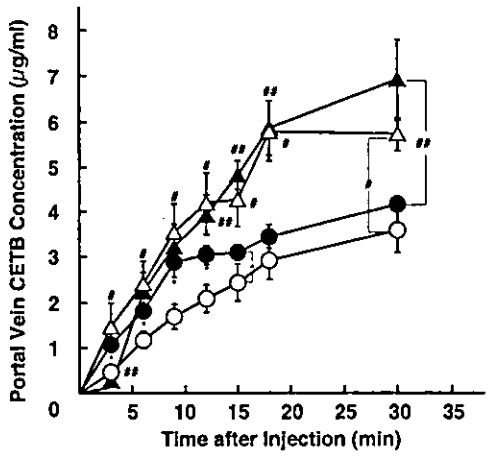

Fig. 7. Time course of portal vein CETB concentration at 8:00 AM and 8:00 PM assessed by in situ duodenum loop techniques in the fed and 4-day fasted rats. ○, 8:00 AM in fed rats; ●, 8:00 PM in fed rats; △, 8:00 AM in 4-day fasted rats; ▲, 8:00 PM in 4 day-fasted rats. Each point represents the mean ± S.E. of five to six rats. *, F0: 8:00 AM versus F0: 8:00 PM; #, F0: 8:00 AM versus F4: 8:00 AM; ##, F0: 8:00 PM versus F4: 8:00 PM. $p < 0.05$, significantly different between each group.

erstein, 1976). In our previous study, we demonstrated that the function and expression of intestinal PEPT1 showed a diurnal rhythm in rat feeding ad libitum (Pan et al., 2002). Because the intestinal PEPT1 diurnal rhythm was also synchronized with food intake, which is one of the major factors regulating of the intestinal PEPT1, the present study was performed to examine the effect of food intake on diurnal variation of intestinal PEPT1 using fed and fasted rats.

The intestinal PEPT1 protein showed significant diurnal rhythm in feeding and 1-day fasted conditions. However, this diurnal rhythm disappeared after 2 days of fasting. In accordance with the diurnal rhythm of PEPT1 protein expression in feeding and fasting conditions, the CETB absorption rate assessed by the in situ loop technique was higher at 8:00 PM rather than at 8:00 AM in the feeding state, but not in the 4-day fasted condition. Interestingly, the diurnal regulation of the PEPT1 mRNA level was maintained even in the 4-day fasted state. This finding suggested that the transcription of intestinal PEPT1 gene in the diurnal rhythm was mediated by factors other than food intake. Currently, there is no information regarding transcription factors involved in the constitutive and regulatory expression of intestinal PEPT1 mRNA. Further studies about promoter analysis of rat PEPT1 may clarify the molecular mechanisms for the diurnal rhythm of intestinal PEPT1 mRNA expression. For Na^+/glucose cotransporter 1, it was demonstrated that periodicity in transcription factor hepatocyte nuclear factor-1 contributes to circadian changes in glucose transport activity in the intestine (Rhoads et al., 1998). Because there is a potential site for HNF-1 in the rat PEPT1 promoter region (Shiraga et al., 1999), this factor can be a candidate for diurnal transcriptional regulation of the intestinal PEPT1 expression.

The diurnal variation of intestinal PEPT1 protein expression was abolished in 4-day fasted rats, although the diurnal variation in the mRNA expression was retained. There are some possible explanations for this finding. First, the rates of the translation process and degradation of PEPT1 protein at 8:00 AM and 8:00 PM may be different between the fed and fasted conditions. Second, the alteration in the cellular distribution of PEPT1 protein (cytoplasmic pool and apical membranes) seems to be involved in the disappearance of diurnal variation. For example, the increased translocation of the cytoplasmic pool of PEPT1 to the apical membrane was demonstrated by hormone treatment such as insulin (Gangopadhyay et al., 2002; Thamotharan et al., 1999) and leptin (Buyse et al., 2001). Insulin and leptin showed a diurnal rhythm with a nocturnal peak, but this rhythm of both hormones was completely abolished by the fasting state (Ahrén, 2000), which seemed to correspond to the alteration of PEPT1 membrane expression between the fed and fasted conditions.

Several clinical studies, performed in a crossover design, have provided evidence that the pharmacokinetics of many lipophilic drugs can be circadian phase-dependent in C_{max} and T_{max} (Lemmer, 1999). Because most drugs tested are absorbed by passive diffusion, the circadian variation in gastric emptying time (Goo et al., 1987) and the perfusion of the gastrointestinal tract (Lemmer and Nold, 1991) have been considered for this reason. In the present study, we found that pharmacokinetic parameters of CETB such as C_{max} and T_{max} showed a significant diurnal variation after intraintestinal administration in fed rats. The initial absorption rate of CETB assessed by the in situ loop technique was significantly higher at 8:00 PM than at 8:00 AM, and pharmacokinetic parameters of intravenous administration of CETB did not show diurnal variation. These findings suggested that pharmacokinetic variation of CETB between 8:00 AM and 8:00 PM was caused by the intestinal absorption process and that the diurnal rhythm of the intestinal PEPT1 expression plays a pivotal role in this variation. The diminished diurnal

TABLE 1

Pharmacokinetic parameters of CETB after intraintestinal administration in fed and 4-day fasted rats at 8:00 AM and 8:00 PM of 1 day

CETB was intraintestinally injected as a dose of 3 mg/kg. Each value represents the mean ± S.E. of four to five rats.

	Fed Rats		4-Day Fasted Rats	
	8:00 AM	8:00 PM	8:00 AM	8:00 PM
T_{max} (min)	42.4 ± 4.6	32.5 ± 2.5[a]	60.0 ± 10.3[b]	54.0 ± 10.2[c]
C_{max} (ml/min/kg)	2.0 ± 0.4	2.7 ± 0.3[a]	4.8 ± 0.7[b]	4.6 ± 0.4[c]
$AUC_{0-3\,h}$ (μg · min/ml)	208.6 ± 20.9	275.4 ± 27.5[a]	599.9 ± 160.9[b]	521.1 ± 99.1[c]

[a] F0: 8:00 AM versus F0: 8:00 PM.
[b] F0: 8:00 AM versus F4: 8:00 AM.
[c] F0: 8:00 PM versus F4: 8:00 PM. $p < 0.05$, significant difference between each group.

TABLE 2

Pharmacokinetic parameters of CETB after intravenous administration in fed and 4-day fasted rats at 8:00 AM and 8:00 PM of 1 day

	Fed Rats		4-Day Fasted Rats	
	8:00 AM	8:00 PM	8:00 AM	8:00 PM
K_e (l/min)	0.029 ± 0.004	0.025 ± 0.000	0.011 ± 0.001[a]	0.014 ± 0.002[b]
$T_{1/2}$ (min)	26.9 ± 2.7	28.1 ± 0.4	67.3 ± 10.0[a]	58.1 ± 19.5[b]
V_d (l/kg)	0.43 ± 0.09	0.40 ± 0.06	0.37 ± 0.06	0.34 ± 0.05
CL_{tot} (ml/min/kg)	10.5 ± 0.6	9.9 ± 1.5	3.8 ± 0.1[a]	4.5 ± 0.7[b]

CETB was intravenously injected as a dose of 3 mg/kg. Each value represents the mean ± S.E. of three rats.
[a] F0: 8:00 AM versus F4: 8:00 AM.
[b] F0: 8:00 PM versus F4: 8:00 PM. $p < 0.05$, significant difference between each group.

variation of the pharmacokinetic parameters for CETB administered intraintestinally in 4-day fasted rats corresponding to the disappearance of the diurnal rhythm of intestinal PEPT1 also supported this idea. As far as we know, this is the first demonstration that the intestinal transporter is involved in the diurnal variation of pharmacokinetics of drugs.

In the intravenous administration, there were no significant differences in pharmacokinetic parameters of CETB

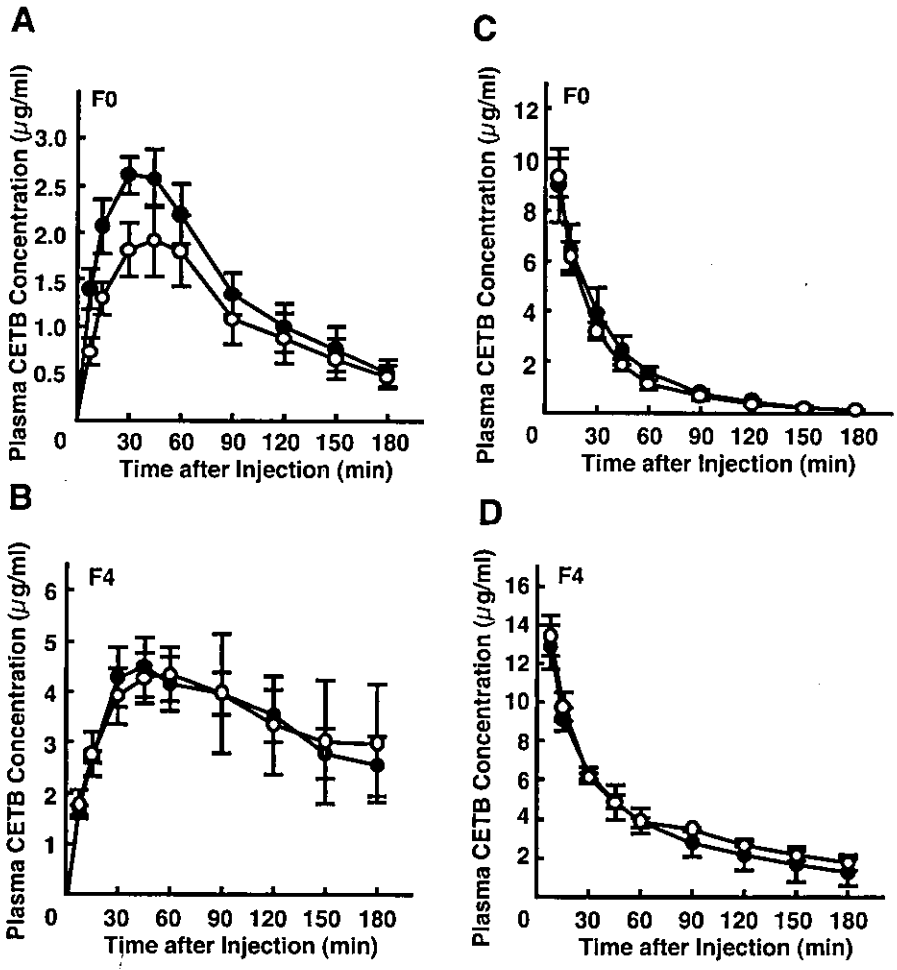

Fig. 8. Effect of fasting on plasma concentration of CETB after intraintestinal (A and B) and intravenous (C and D) administration in fed and 4-day fasted rats at 8:00 AM and 8:00 PM of 1 day. CETB was injected at single dose of 3 mg/kg at 8:00 AM or 8:00 PM. Blood samples were collected at the specified times after the injection. ○, dosing at 8:00 AM; ●, dosing at 8:00 PM. Each point represents the mean ± S.E. of six (A and B) or three (C and D) rats. *, $p < 0.05$, significantly difference between each group.